MODEL OF THE SELF-ASSEMBLY PROCESS OF DIELECTRIC NANOSPHERES DEPOSITED BY ELECTROSPRAY

Davide Padoan

Candidate: Davide Padoan .....
Spanish supervisor: Luis Castañer .....
Italian supervisor: Danilo Demarchi .....

A thesis presented for **double degree** of
Electronic Engineering

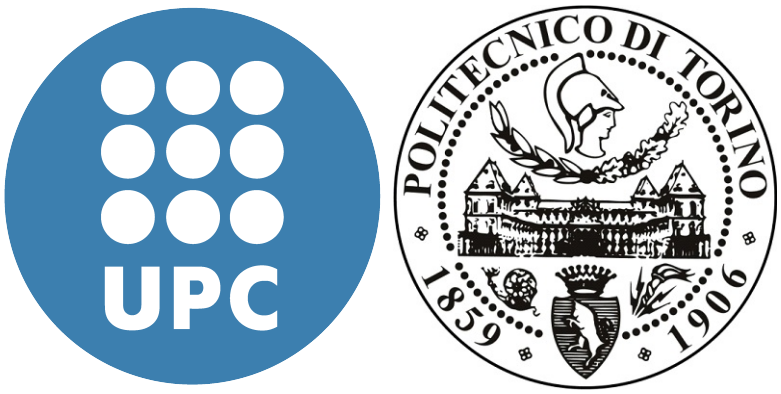

Universitat Politecnica de Catalunya / Politecnico di Torino
Barcelona / Torino
2014/05/21

A i miei genitori,
che, nonostante i tempi bui,
hanno sempre intravisto la luce.

A Luis y a Sandra,
que, con sus paciencia,
me han acompañado en el camino de mi futuro.

Contents

1 Introduction & motivation

In recent years nanotechnology has impacted many research domains and industries to master the nanodimensions to taylor surfaces, materials and properties. In many ocasions, nanoparticles and coatings or devices based on them shown interesting new properties or functionalities.
In biology, for example, nanospheres are used in order to build filters that are capable to catch particular bacteria or cells, to make possible a better analysis of the particle selected. So, it is possible, for example, analyze the DNA, in order to detect some blood's anomalies [1]. Another way to use nanospheres filters is to protect the liquid from some particular bacteria, for example in the case of water's filter [2][3]. In MEMS (Micro Electro-Mechanicals Systems) as in NEMS (Nano Electro-Mechanical System) often nanoparticles are used technnology [4][5]. Recently, nanoparticles technology are also used to fight cancer [6]. The nanospheres are also used in textile field, where it has been discovered that, using polymer's nanospheres, it is possible to create a new type of tissue hydrofobic, antibacterial, anti odor and stain resistance[7]. The Schoeller industries, for example, use the nanosphere technology in order to create different wear products, in special case it is ideal for use in clothing for such areas as outdoor, sportswear, men's fashion,women's wear, career apparel and workwear as well as for shoes and home furnishings.

This technology worked because the nanospheres are regularly organized or self-assembled. In order to make this possible, there are many approaches. We can cite some of them [8]:

1. Drop coating: the actractive capillary force and convective transport af the nanospheres arising from the continuous solvent evaporation are the main factors dominating the self-assembly process, and the ordering and quality of the obtained arrays are largely determined by the evaporation rate.

2. Dip coating: The substrate is immersed in the solution of the coating material at a constant speed. The thin layer deposit itself while it is pulling up. Excess liquid will drain from the surface and then the solvent evaporates from the liquid [9];

3. Spin coating: A small amount of coating material is applied on the center of the substrate. The substrate is then rotated at high speed in order to spread the coating material by centrifugal force [10];

4. Electrophoretic deposition: a thin layer of colloidal suspension is confined between two electrodes, and an applied electric field drives the charged nanospheres to move towards the electrodes, leading to their self-assembly on the electrode interfaces [11].

With those approaches it is also possible to create a new type of materials, known as **metamaterials**, that, combinating nanosphere of differents materials in a specific geometric position, have properties difficult to find in nature. One of the most interesting properties discovered it is about optics issues [12] [13]. In fact, using specific components and a well defined nanosphere geometry, it is possible create a material able to have a negative refraction index, impossible to find in nature. That discovery opened the world at the **superlenses** that can greatly increase optical resolution beyond the capability of conventional lenses, becoming a solution to the centuries old problem of diffraction-limited systems.In other work, a form of **invisibility** has been demonstrated at least over a narrow wave band. Although the first metamaterials were electromagnetic, acoustic and seismic metamaterials are also areas of active research. Potencial application of metamaterials are diverse and include remote aerospace applications, sensor detection and infrastructure monitoring, smart solar power management, public safety, radomes, high-frequency battlefield communication and lenses for high-gain antennas, improving ultrasonic sensor, and even shielding structures from earthquakes. The research in metamaterials is interdisciplinary and involves such fields as electrical engineering, electromagnetics, solid state physics, microwave and antennas engineering, optoelectronics, classic optics material sciences, semiconductor engineering, nanoscience and others.

One of the best techniques used to manipulate nanoparticles is with the help of an electric field [14]. Recently, several attempts to use dielectrophoresis (DEP) as a novel method for nanoparticles manipulation have been made. This force does not require the particle to be charged, the strength of the force depends strongly on the medium and particles' electrical properties, on the particles' shape and size, as well as on the frequency of the electric field. Thus, under the action of spatially non-uniform AC electric fields, dielectric particles move. DEP methods can be used in many forms (electrorotation, traveling wave DEP, negative and positive DEP) to manipulate and more generally, to control the position, orientation and velocity of micro- and nanometric scale particles, including carbon nanotubes and biological particles such as viruses, DNA, bacteria and cells of various kinds (mass spectrometer [15]). Since the relative dielectric polarization (and hence the dielectric response) of the nanoparticles depends on the driving frequency of the applied electric field, an alternating (AC) electric field is usually applied to generate DEP forces of different magnitudes and directions.

In order to make possible the nanoparticle manipulation, we must allocate the nanosphere in the middle of the plates. One of the methods most known to do this is using the **electrospray method** [16] [17]. The way it works is simple: we use a plane of metal (cathode), for example aluminium, and a needle (anode), in which one there is a liquid (water or alcohol) full of nanospheres in suspension, in our case polystyrene nanospheres. If we apply between the needle and the plane a electric field sufficiently high, it

is formed the **Tailor Cone**, well explained in chapter 3.1, on the tip of the needle, causing so a jet of liquid that, depending of the intensity of the electric field, generate a spray.

In this project we work on an analytical solution for the dielectrophoretic force in an electrospray experiment , creating a model with MATLAB, in order to understand better the behavior of the nanosphere under electrospraying method and dielectrophoretic force (DEP), with special regard for the self-assembly effect.

2 Schwarz-Christoffel mapping and electric field calculation

In this section we describe the calculation of the electric field distribution in a simplified geometry of the electrospray technique consisting in a needle where the nanofluid is injected with the help of a microflouidic pump and a substrate. Figure 1 shows the schematic diagramme of the geometry.

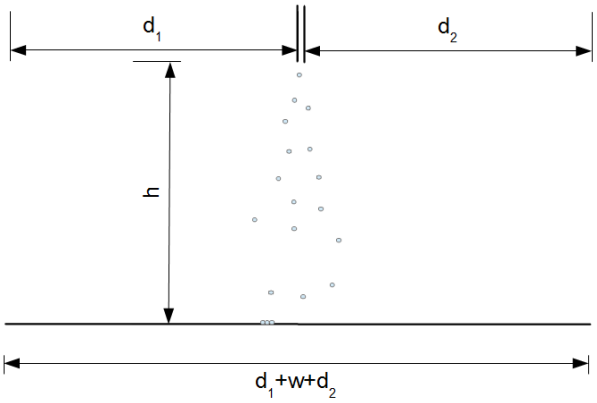

Figure 1: Schematic diagramme

For the calculation of the electric field we have considered a simplified geometry as shown in Figure 2

2.1 Fundamental of Schwarz-Christoffel transformation

We have used the Schwartz-Christoffel approximation [18] starting in the Z-plane shown in Figure 2

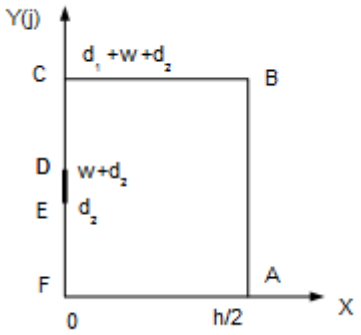

Figure 2: Z-plane

where we have 6 characteristic points : D and E are the edges of the

needle where the voltage is applied, FA distance is taken half of the real distance needle-ground plane, due to the simmetry of the system, while the points A and B are the edges of the ground plane and C and F are their projections in the DE line. The Z-plane is a complex version of the physical plane rotated 90°in such a way that the imaginary axis corresponds to the plane where the needle is located and the real axis corresponds to the distance from the needle (*Figure 2*).

Before applying the SC transformation to our case , let us review the basics in the general case of a closed polygon as shown in Figure 3.

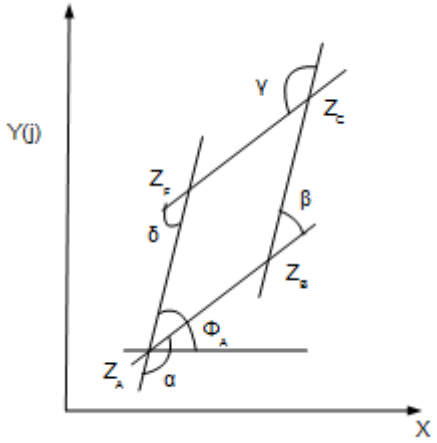

Figure 3: Z-plane general case

Any point in the Z-plane may be identified by vector. In the example shows in Figure 3, we travel counterclockwise around the closed polygon and, according to the angle definition shown in Figure 3, the distance $(Z - Z_A)$ before and after point A can be written as:

$$\begin{aligned} before \qquad & Z - Z_A = |Z - Z_A| e^{j\phi_A} \\ after \qquad & Z - Z_A = |Z - Z_A| e^{j[\phi_A - (\pi - \alpha)]} \end{aligned}$$

where ϕ_A is the angle between the horizontal axis and the polygon side by the point into consideration and the previous point, in our case, Z_F, and α is the angle between the extension of the line constructed by the point into consideration and the previous point and the line constructed by the point into consideration and the following point, Z_B in our case (*Figure 3*).

Once the Z-plane has been established the SC transformation consists in mapping the points inside the closed polygon into a new T-plane in such a way that all corner points of the Z-plane polygon are mapped onto points in the real axis of the T-plane as shown in Figure 4.

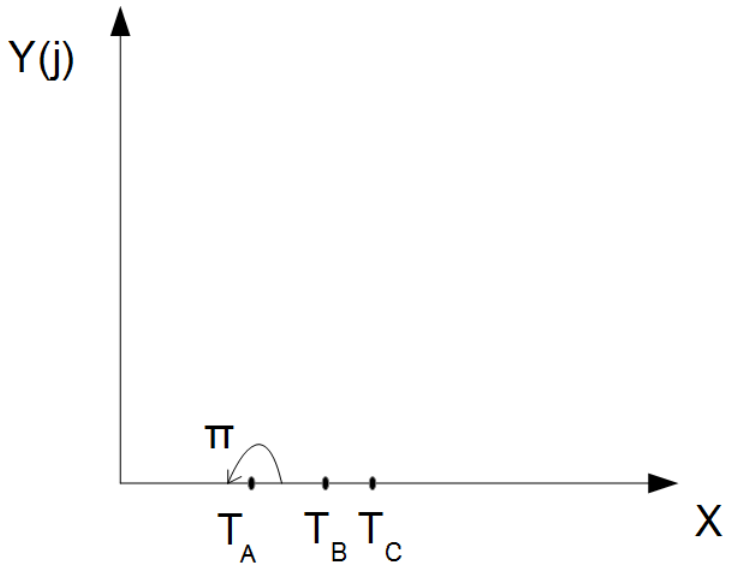

Figure 4: T-plane

Now the travel around the polygon in the Z-plane is transformed in a travel along the real axis in the T-plane where the distances around one of the points, for example T_A, can be written as :

$$\begin{aligned} before \qquad & T - T_A = |T - T_A| e^{j\pi} \\ after \qquad & T - T_A = |T - T_A| e^{j0} \end{aligned}$$

Now, the mapping from Z-plane into T-plane can be written as,

$$Z - Z_A = (T - T_A)^{\frac{1}{p}}$$

and the corrispondence of distances is

$$\begin{cases} |Z - Z_A| e^{j\phi_A} & = |T - T_A| e^{j\frac{\pi}{p}} \\ |Z - Z_A| e^{j[\phi_A - (\pi - \alpha)]} & = |T - T_A| e^{j\frac{0}{p}} = |T - T_A| \end{cases} \tag{1}$$

Comparing equations (1):

$$\frac{1}{p} = 1 - \frac{\alpha}{\pi}$$

so the vectors Z and T are related by

$$\begin{aligned} Z &= C T^{1-\frac{\alpha}{\pi}} \\ \frac{dZ}{dT} &= C\left(1 - \frac{\alpha}{\pi}\right) T^{1-\frac{\alpha}{\pi}-1} \\ \frac{dZ}{dT} &= C_1 T^{-\frac{\alpha}{\pi}} \qquad where \qquad C_1 = C\left(1 - \frac{\alpha}{\pi}\right) \end{aligned}$$

In the case of four corners

$$\frac{dZ}{dT} = C_1 |T - T_A|^{-\frac{\alpha}{\pi}} |T - T_B|^{-\frac{\beta}{\pi}} |T - T_C|^{-\frac{\gamma}{\pi}} |T - T_F|^{-\frac{\delta}{\pi}} \tag{2}$$

2.2 Schwarz-Christoffel application to the electrospray geometry

Applying Eq.(2) to the electrospray geometry shows in Figure (2) and as the polygon in the Z-plane has all corners rectangular $\alpha = \beta = \gamma = \delta = \frac{\pi}{2}$ we find that [19]

$$Z = C_1 \int \frac{dT}{\sqrt{(T - T_A)(T - T_B)(T - T_C)(T - T_F)}} \tag{3}$$

Equation (3) can be transformed after variable change in an elliptic integral [20]

$$Z = C_3 F(\omega_1, k_1) + C_2 = C_3 \int_0^{\lambda_1} \frac{d\lambda_1}{\sqrt{(1 - \lambda_1^2)(1 - k_1^2 \lambda_1^2)}} + C_2 \tag{4}$$

where

$$\begin{aligned} C_3 &= \frac{2C_1}{\sqrt{(T_F - T_B)(T_C - T_A)}} \\ \omega_1 &= \arcsin\left[\sqrt{\frac{(T_C - T_A)(T - T_F)}{(T_F - T_A)(T - T_C)}}\right] \\ k_1 &= \sqrt{\frac{(T_C - T_B)(T_F - T_A)}{(T_F - T_B)(T_C - T_A)}} \\ \lambda_1 &= \sin\omega_1 \end{aligned} \tag{5}$$

where $F(\omega_1, k_1)$ is the elliptical integral of the first kind and k_1 is the modulus of the elliptic function.
Equation (4) links the T plane to the Z plane. The values of the coefficients C_2 and C_3 can be solved by the mapping relationship between the coordinates of the corresponding points in the two planes ($Z_F \to T_F, Z_C \to T_C, Z_B \to T_B, Z_A \to T_A$) leading to,

$$\begin{aligned} C_2 &= 0 \\ C_3 &= \frac{h}{2K(k_1)} = \frac{d_1 + w + d_2}{K(k_1')} \end{aligned}$$

where $K(k_1)$ is the complete elliptic integral of the first kind and $k_1' = \sqrt{1 - k_1^2}$.
In this manner, it can be written like

$$\frac{dZ}{dT} = \frac{h}{2K(k_1)} \frac{\sqrt{(T_F - T_B)(T_C - T_A)}}{2\sqrt{(T - T_A)(T - T_B)(T - T_C)(T - T_F)}} \tag{6}$$

After the mapping into the T-plane has been completed, a second mapping is performed between the T-plane and a new W plane, in such a way

that the points in real axis in the T-plane are mapped now onto a new closed polygon as shown in Figure 5.
The reason for this transformation is to get a parallel plate geometry where the boundary conditions are the known potential at the two plate and the Dirichlet boundary condition (continuity of potential and electric field) at the two lateral side.

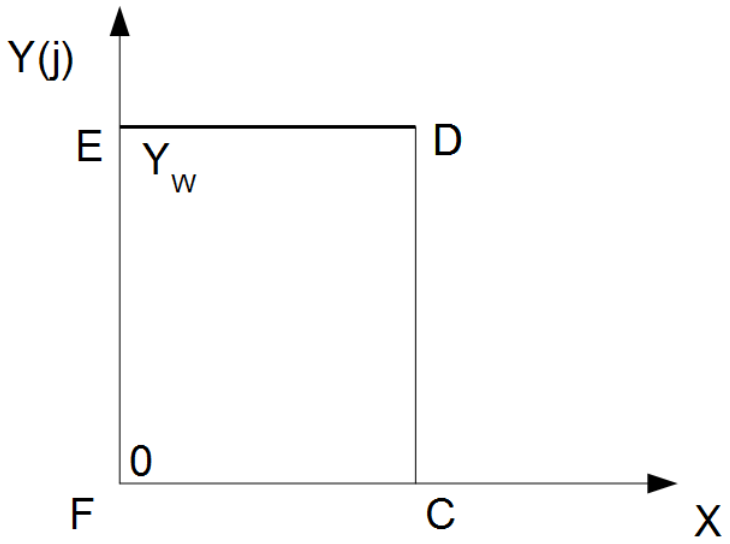

Figure 5: W-plane

The second SCM is used to transform the upper half of the T-plane into a rectangle in the model plane (W-plane). The electric field is uniformly distribuited in the interior of the rectangle due to the restriction from the transformed boundaries in the W-plane. The corrisponding points are $W_E = jY_W$, $W_D = X_W + jY_W$, $W_C = X_W$ and $W_F = 0$, where X_W and Y_W are the size of the rectangle along the real and immaginary axes, respectively. Similarly, the transformation from the T-plane to the W-plane is given by

$$W = D_1 \int \frac{dT}{\sqrt{(T - T_C)(T - T_D)(T - T_E)(T - T_F)}} \tag{7}$$

that after variable change also transforms in an elliptic integral

$$W = D_3 F(\omega_2, k_2) + D_2 = D_3 \int_0^{\lambda_2} \frac{d\lambda_2}{\sqrt{(1 - \lambda_2^2)(1 - k_2^2\lambda_2^2)}} + D_2 \tag{8}$$

with

$$
\begin{aligned}
D_3 &= \frac{2D_1}{\sqrt{(T_F - T_D)(T_E - T_C)}} \\
\omega_2 &= \arcsin\left[\sqrt{\frac{(T_E - T_C)(T - T_F)}{(T_F - T_C)(T - T_E)}}\right] \\
k_2 &= \sqrt{\frac{(T_E - T_D)(T_F - T_C)}{(T_F - T_D)(T_E - T_C)}} \\
\lambda_2 &= \sin\omega_2
\end{aligned}
\tag{9}
$$

Equation (8) links T plane with the W plane. The values of the coefficients D_2 and D_3 can be obtained by a similar mapping procedure to the first SCM performance.

$$
\begin{aligned}
D_2 &= 0 \\
D_3 &= \frac{Y_W}{K(k_2')}
\end{aligned}
$$

where Y_W is the lenght of the side of the rectangle along the imaginary axis. So, we can write that

$$
\frac{dW}{dT} = \frac{Y_W}{2K(k_2')} \frac{\sqrt{(T_F - T_D)(T_E - T_C)}}{\sqrt{(T - T_C)(T - T_D)(T - T_E)(T - T_F)}} \tag{10}
$$

Now, to find the electric field in the Z plane and, as the Laplace equation is conserved in the transformation,

$$
\nabla\phi_Z = \nabla\phi_W \overline{f'(Z)} = \nabla\phi_W \overline{\frac{dW}{dZ}} \tag{11}
$$

with

$$
\begin{aligned}
\nabla\phi_W &= j\frac{V}{Y_W} \\
\frac{dW}{dZ} &= \frac{dW}{dT}\frac{dT}{dZ}
\end{aligned}
$$

so, we find that the electric field is calculated as

$$
E_0 = \nabla\phi_Z = \overline{j\frac{2V}{h}\frac{K(k_1)}{K(k_2')}\frac{\sqrt{(T_F - T_D)(T_E - T_C)(T - T_A)(T - T_B)}}{\sqrt{(T_F - T_B)(T_C - T_A)(T - T_E)(T - T_D)}}} \tag{12}
$$

This is the main result of the SC transformation applied in the electrospray geometry and provides an analytical solution for the electric field at any point inside the original polygon in the physical domain.

The SC transformation has several degrees of freedom and up to three values for the points in the T-plane can be arbitrarily chosen following this criteria [18]:

$$T_F > T_E > T_D > T_C > T_B > T_A$$

where T_A is chosen to be equal to 0.

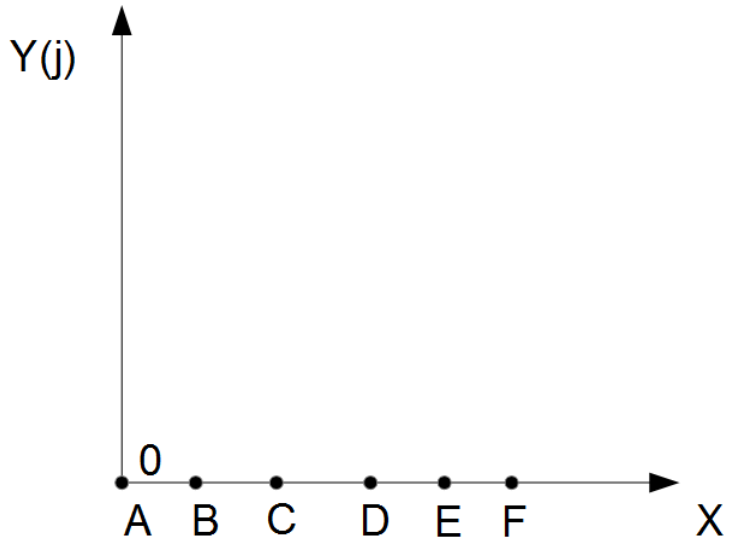

Figure 6: T-plane

To choose the points T_B and T_C, we know that

$$T_F > 0 \qquad \text{and hence} \qquad k_1^2 > 1 - \frac{T_B}{T_C}$$

where k_1 is the modulus of the elliptic function. In order to calculate this coefficient, we use the **Hilberg**'s approximations [21]:

$$M = \frac{1}{4} e^{\frac{h\pi}{2(d_1+w+d_2)}} \qquad \text{if} \qquad \frac{K(k_1)}{K(k_1')} \geq 1$$

$$M = \frac{1}{4} e^{\frac{2\pi(d_1+w+d_2)}{h}} \qquad otherwise$$

where $K(k_1)$ is the complete elliptic integral of the first kind and $k_1' = \sqrt{1-k_1^2}$. From those equations, we can finally obtain the value of T_B and T_C. Choosing $T_B = 1$, we find $T_C = 1.0009$.

From equation (5),we can calculate T_F:

$$T_F = \frac{T_B(T_C - T_A)k_1^2 - T_A(T_C - T_B)}{(T_C - T_A)k_1^2 - (T_C - T_B)} \tag{13}$$

To find the other points in the plane T, we use the inverse function of Eq.(4)

$$T = \frac{T_F T_C cn^2(\frac{Z}{C_3}, k_1)}{T_C - T_F sn^2(\frac{Z}{C_3}, k_1)} \tag{14}$$

where cn and sn are the `Jacobian elliptic functions` and $C_3 = \frac{h}{2K(k_1)}$. With equation (14), we can find the value of T_D and T_E.

$$T_D = \frac{T_F T_C cn^2(j\frac{w+d_2}{C_3}, k_1)}{T_C - T_F sn^2(j\frac{w+d_2}{C_3}, k_1)} \tag{15}$$

$$T_E = \frac{T_F T_C cn^2(j\frac{d_2}{C_3}, k_1)}{T_C - T_F sn^2(j\frac{d_2}{C_3}, k_1)} \tag{16}$$

Now that we have find all the points in the plane T, we can calculate the electric field in the Z plane with Eq.(12).

Figure (7) shows the electric field value at different distances from the needle, for an applied voltage of $10000V$, distance between electrodes $h = 10cm$, diameter of the needle $w = 0.3mm$, distance between the needle and the end of the collector plane $d_1 = d_2 = 4.985cm$.

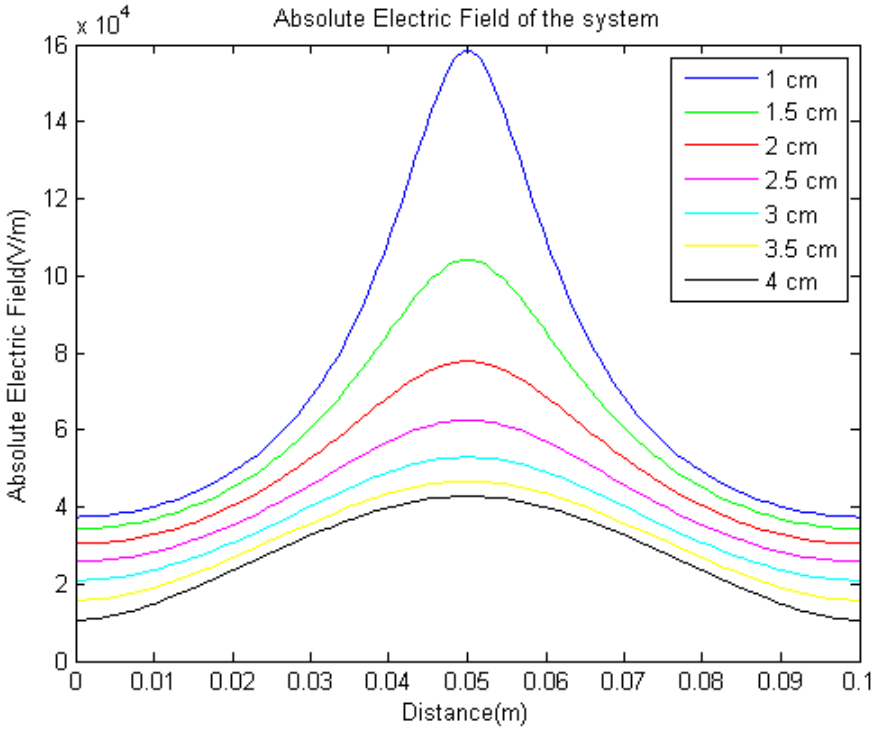

Figure 7: Absolute Electric Field

As we can see in Figure (7), the order of magnitude of the electric field value is in the $10^5 \frac{V}{m}$ range and, more we get closer to the substrate, the electric field becomes smaller. Moreover, we can say that not only becomes smaller, but tends to become constant along the x-axis, but has a gradient along the y-axis, as we can see in Figure (8) and (9).

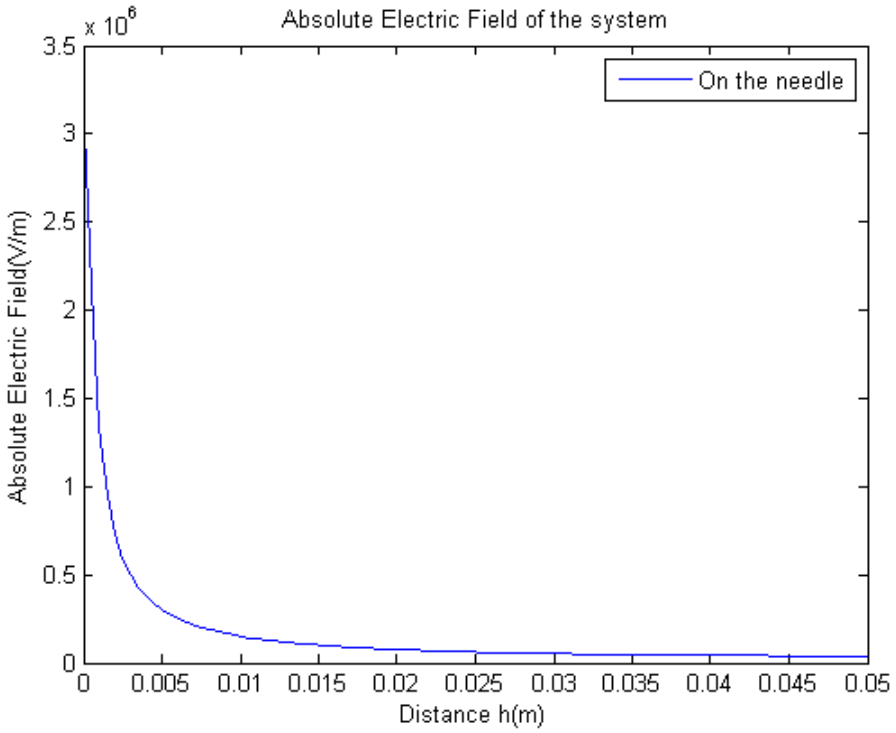

Figure 8: Absolute Electric Field on the needle

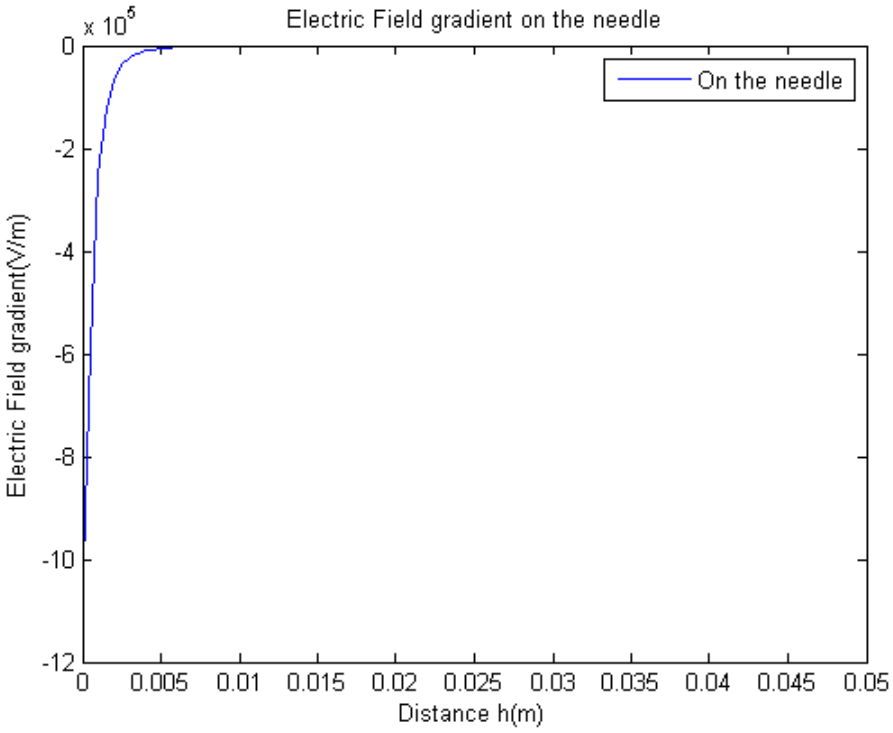

Figure 9: Electric Field gradient

The reason why the electric field is not constant near to the needle is because we are not using two plate to induce the electric field, but a plate and a needle.

In order to understand better the behavior of the electric field, let's change some parameters. For example, if we change the diameter of the needle, the magnitude of the electric field becomes higher and its distribution becomes wider while we increase the diameter dimension (Figure (10)).

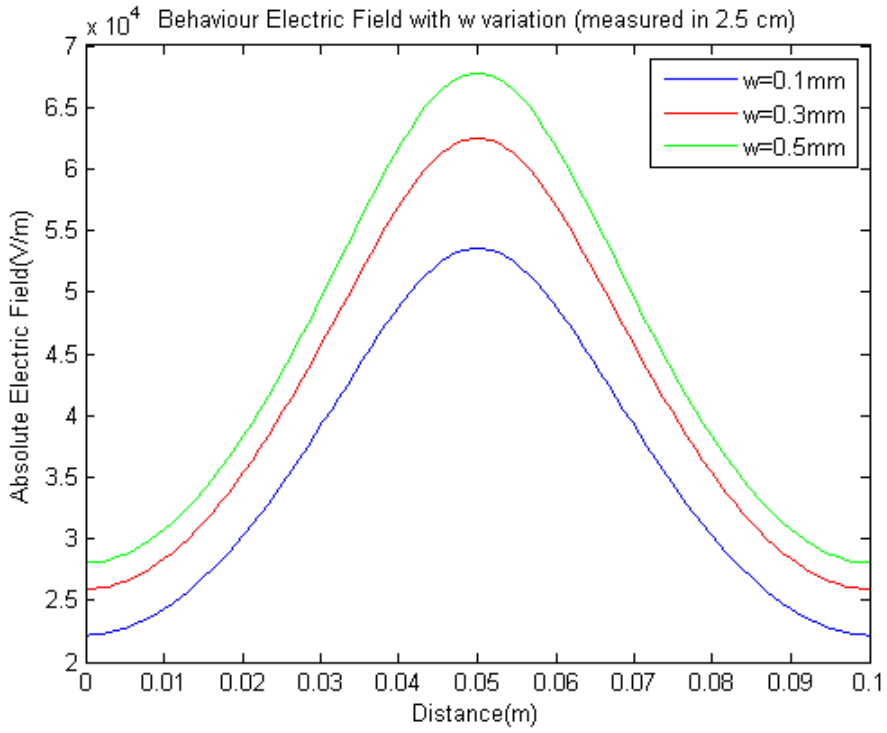

Figure 10: Behaviour of the electric field as a function of the needle diameter , w

Instead, if we increase the distance between the needle and the ground plate, we found that the magnitude of the electric field decreases (Figure (11)). That means that the distance h is inversely proportional to the electric field, as we can see in equation (12).

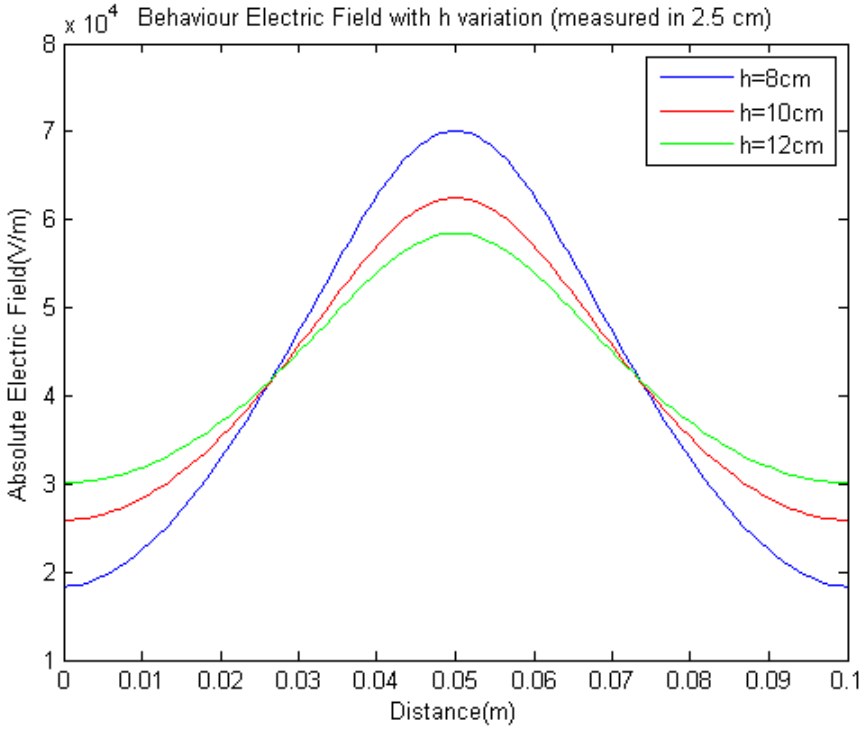

Figure 11: Behaviour of the electric field by variating h parameter

Another parameter to take to account is the magnitude of the electric field near at the needle. This is shown in figure (12), where it can be seen that the electric field close to the needle edge at the needle is about $3.14 * 10^6 \frac{V}{m}$, that means that at the tip of the needle the high value of the field can create a phenomenon called Taylor's cone [22] as discussed in the following chapter.

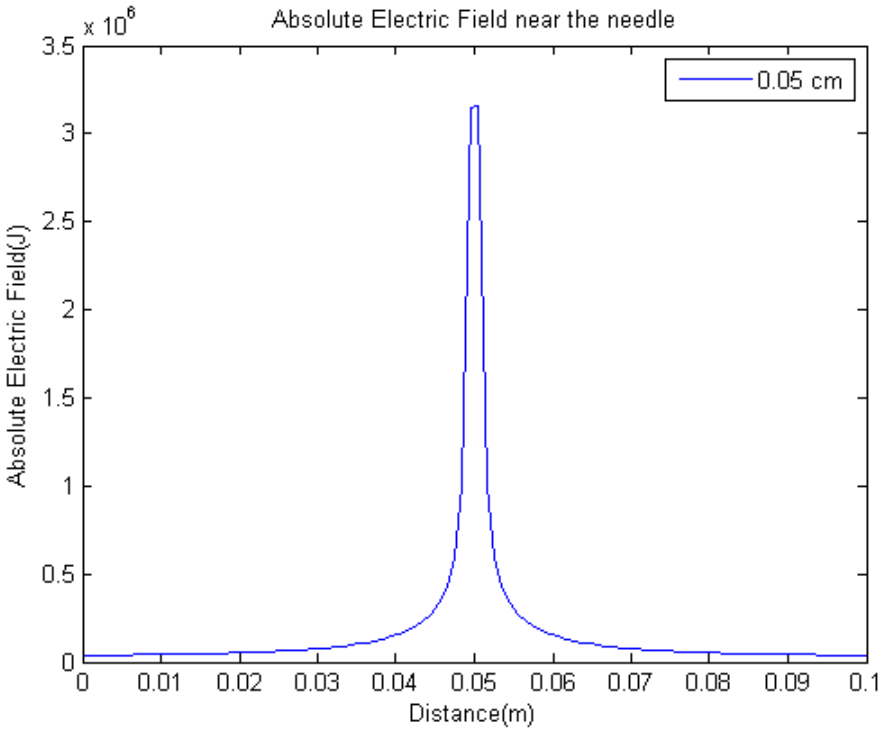

Figure 12: Absolute Electric Field near the needle

3 Electrospray process and phases

Our hypothesis of the electrospray deposit process involves three main phases:

1. **Ejection phase of droplets**
2. **Droplet travel towards the substrate**
3. **Landing and drying phase**

3.1 Ejection phase, Taylor cone and droplet charge

When a small volume of electrically conductive liquid is exposed to an electric field, the shape of liquid starts to deform from the shape caused by surface tension alone. As the voltage increases, the electric field exerts a similar amount of force on the droplet as the surface tension does; a cone shape begins to form with convex sides and a rounded tip. This approaches the shape of a cone with a whole angle of $98.6°(\theta = 49.3°)$[23]. When a certain threshold voltage has been reached, the slightly rounded tip emits a jet of microdroplets called a *conejet* and is the beginning of the electrospraying process in which ions may be transferred to the gas phase. It is generally found that in order to achieve a stable conejet a slightly higher than threshold voltage must be used. As the voltage is increased even more, other modes of droplet desintegration are found.

The threshold voltage that sets the Taylor cone, is found from equations[23],

$$r_{drop} = \left(\frac{\rho}{4\pi^2 \gamma \tan(\frac{\pi}{2} - \theta)[(\frac{U_a}{U_T})^2 - 1]} \right)^{1/3} \times \left(\frac{dV}{dt} \right)^{2/3} \tag{17}$$

$$U_T = 0.863 \left(\gamma \frac{h}{\varepsilon_0} \right)^{1/2} \tag{18}$$

$$q_{drop} = 8\pi \left(\varepsilon_m \gamma r_{drop}^3 \right)^{1/2} \tag{19}$$

$$F_{drop} = q_{drop} |E_0| \tag{20}$$

where r_{drop} is the radius of the water's drop, that is equal to the radius of the tip of the Taylor's cone, U_T is the threshold voltage, U_a is the applied voltage, γ is the surface tension of the liquid, θ is the liquid cone angle (supposed equal to 49.3°for the classical Taylor cone model), ρ is the density of the liquid, $\frac{dV}{dt}$ is the flow rate, ε_0 is the vacuum permittivity and h is the distance between needle and substrate.

So, theorically, if we use water ($\gamma = 0.073$) with a distance $h = 10cm$ we find that we can reach the Taylor cone if we apply a tension higher than 19kV. However, in the experiment described in [24], it is formed at a lower voltage, tipically 8kV. That means that the theoretical value of threshold voltage apparently does not describe accurately the experiment [23].

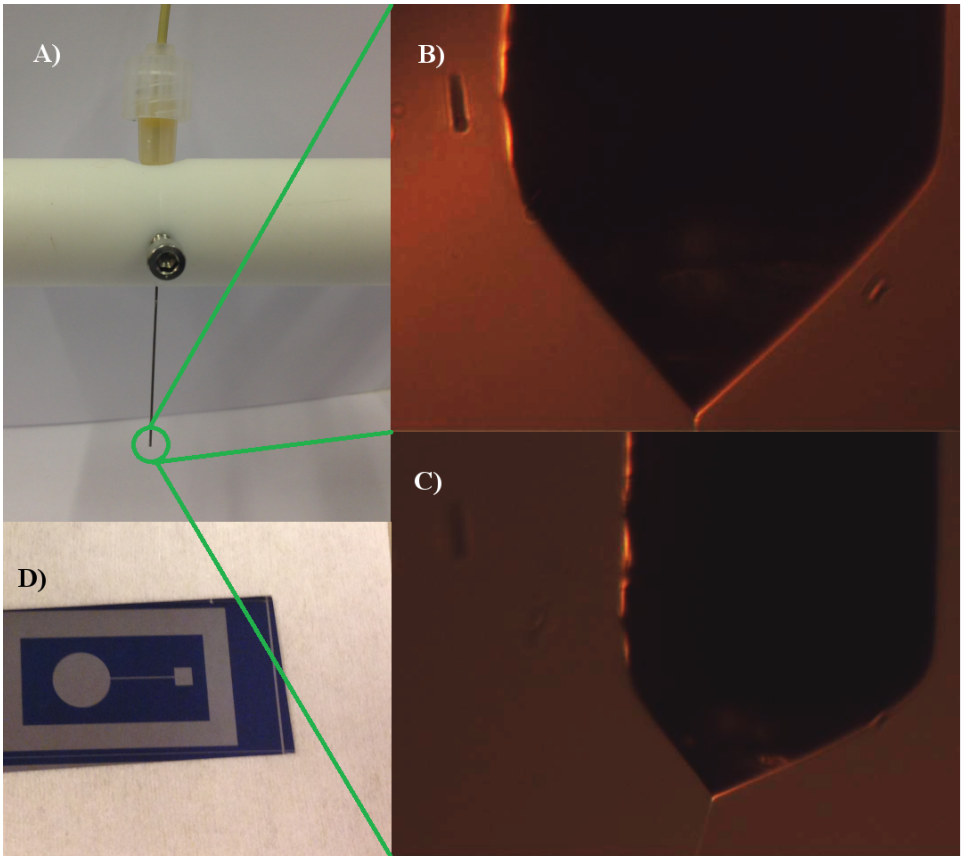

Figure 13: Empirical Taylor cone

In figure 13 shows a picture of the Taylor cone when a tension around to 10kV is applied. In fact, we can see that the angle of the Taylor cone is equal to $87°(\theta = 43.5°)$, clearly below that critical angle. When a droplet is created, it has a dimension defined by the $r_{drop} = 7.57\mu m$ calculated from equation(17). In the experiment registred in [24] spheres of 180nm radius are used and hence we can estimate that in a single droplet can hold more than $3 * 10^4$ particles.

It is well known that the microdroplets after they are ejected, they start loosing liquid as it evaporates more importantly if there is alcohol involved in the solution and hence the droplets are becoming more and more small. So we can take into account two extreme hypothesis:

1. *The liquid has **not** yet evaporated totally*: we have a charged drop of liquid, hence subject to Coulomb Force

2. *The liquid is totally evaporated*: we then assume that the nanospheres, which are dielectric, have to be subject to a Dielectrophoretic Force as they are charge-neutral.

Knowing the electric field, we can calculate the forces that this electric field creates on the droplets or particles. On the one side we have the Coulomb force which is simply proportional to the charge and to the electric field value and that is the main component for charged particles, but we also have the Dielectrophoretic force that appears in dielectric spheres polarized under an electric field. This Dielectrophoretic force is proportional to the gradient of the electric field module squared as follows,

$$F_{DEP} = 2\pi\varepsilon_m R^3 k \nabla |E|^2 \tag{21}$$

where

$$k = Re\left[\frac{\tilde{\varepsilon_p} - \tilde{\varepsilon_m}}{\tilde{\varepsilon_p} + 2\tilde{\varepsilon_m}}\right] \tag{22}$$

is the Clausius-Mossoti Factor, where $\tilde{\varepsilon_p}$ is the polystyrene's permittivity while $\tilde{\varepsilon_m}$ is the air's permittivity.

The Coulomb force's exerted on the droplets ejected is shown in Figure(14) and that of the Dielectrophoretic force direction on a single particle at several distances from the needle is shown in Figure(15).

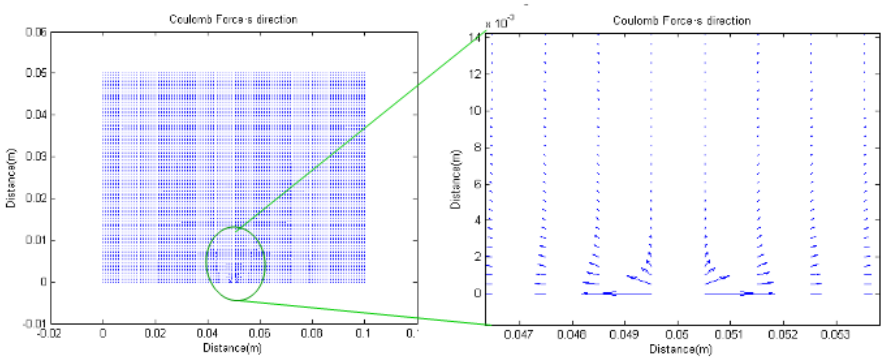

Figure 14: Coulomb's Force's direction

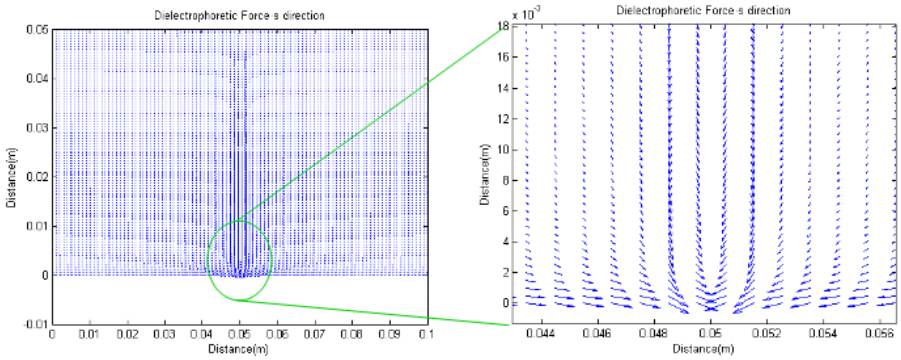

Figure 15: Dielectrophoretic's Force's direction

As can be seen the direction of Coulomb force and Dielectrophoretic force are opposite. Moreover Figure(16) shows the modulus of the two forces. Notice that the distance in vertical axes, 0 is near the needle and 0.05 is far from the needle.

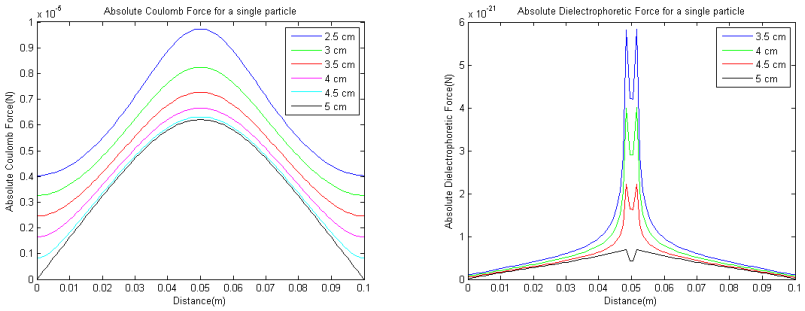

(a) Coulomb's Force (b) Dielectrophoretic Force

Figure 16: Comparison between two forces

If we compare the Coulomb force with the Dielectrophoretic force, we notice that the Coulomb force is many orders of magnitude stronger than the Dielectrophoretic force. An interpretation of this results is that the Dielectrophoretic force is negligeable compared to the Coulomb force and hence in the ejection an travelling phase the droplets are driven towards the substrate by the Coulomb force and that the Dielectrophoretic force, will only be significant if the particles are not inside a droplet because it has dried.

4 Landing and drying phase

4.1 Dielectrophoretic force between two particle

The landing phase is characterized by the deposition of droplets containing nanoparticles on top of the substrate. The observation made in [24] show that several things may happen. On the one hand when the electrically charged droplets fall into the substrate electrode, the electrical charge is collected by the electrode and contributes to the external current in the circuit. Besides, a droplet in the process of drying suffers from the well known effect of "Coffee stain" and the nanoparticles associate randomly due to capillary forces.

However we can make the hypothesis that the nanoparticles are almost free of liquid, beside the intersticial water due to the humidity and can be subject of DEP force.

So we can imagine as a very simple first case, the forces between two dielectric nanoparticles polarized by a constant electric field that are close to each other.

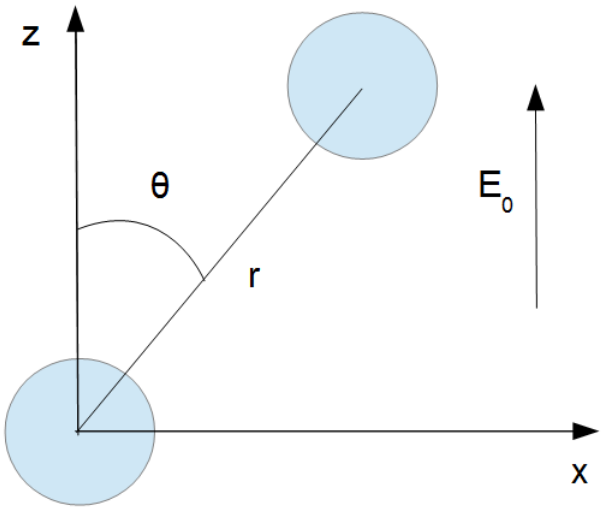

Figure 17: Electrical dipole

For doing this, it's better working with polar coordinates (r, θ), in two dimensions where r is the distance between centers of particles while θ is the angle between them.

In the geometry considered we have a constant electric field in the z-direction and an electric dipole originated by the polarization of the nanoparticle sitting at the origin of coordinates,

4.2 Potential created by a constant electric field

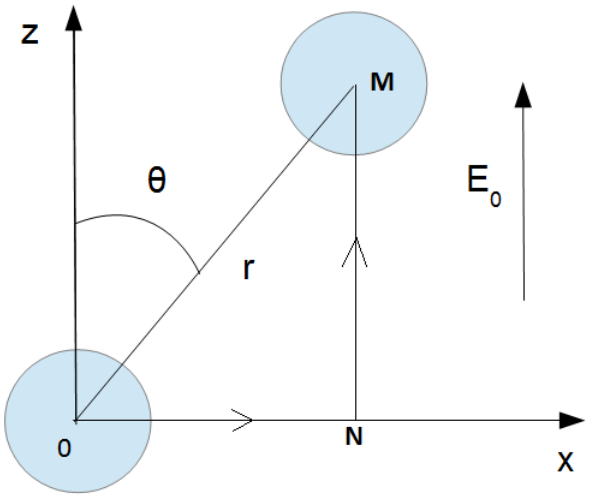

Figure 18: Electrical dipole

Taking into account only the constant electric field, we can calculate the electric potential as,

$$V = -\int_0^M \vec{E}\,\vec{dl} \tag{23}$$

we can divide this integral in two parts,

$$V = -\cancel{\int_0^N \vec{E}\,\vec{dl}} - \int_N^M \vec{E}\,\vec{dl} \tag{24}$$

The first part of the second term is zero because the electric field is orthogonal to the x-axis as it has the direction of Z-axis. So, we find that

$$V = -E_0 r\cos\theta \tag{25}$$

4.3 Potential created by an electrical dipole

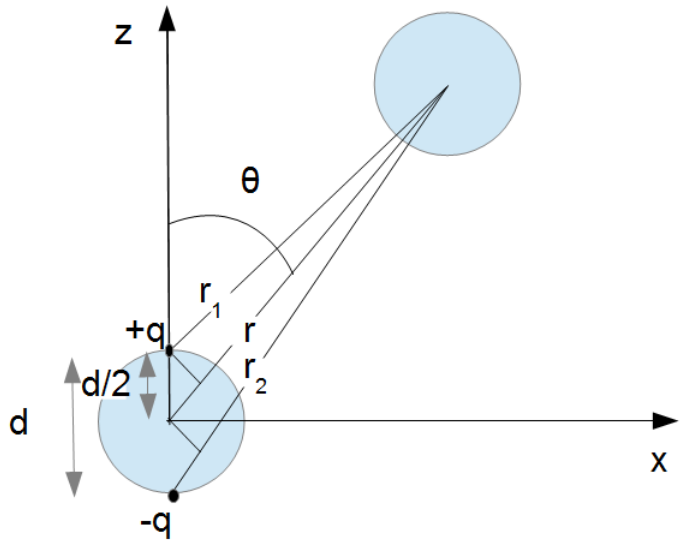

Figure 19: Electrical dipole

Taking into account now only the electrical dipole, we can calculate the electric potential at a distance r from the origin,

$$V = \frac{q}{4\pi\varepsilon_0 r_1} - \frac{q}{4\pi\varepsilon_0 r_2} = \frac{q}{4\pi\varepsilon_0}\left(\frac{1}{r_1} - \frac{1}{r_2}\right) \tag{26}$$

Using the triangle equation, we can say that

$$r_1^2 = r^2 + \left(\frac{d}{2}\right)^2 - rd\cos\theta \tag{27}$$

$$r_2^2 = r^2 + \left(\frac{d}{2}\right)^2 + rd\cos\theta \tag{28}$$

in this manner, we have that

$$V = \frac{q}{4\pi\varepsilon_0}\left(\frac{1}{\sqrt{r^2 + \left(\frac{d}{2}\right)^2 - rd\cos\theta}} - \frac{1}{\sqrt{r^2 + \left(\frac{d}{2}\right)^2 + rd\cos\theta}}\right) \tag{29}$$

$$V = \frac{qd}{4\pi\varepsilon_0}\left(\frac{\frac{1}{d}}{\sqrt{r^2 + \left(\frac{d}{2}\right)^2 - rd\cos\theta}} - \frac{\frac{1}{d}}{\sqrt{r^2 + \left(\frac{d}{2}\right)^2 + rd\cos\theta}}\right) \tag{30}$$

$$V = \frac{qd}{4\pi\varepsilon_0} f(r, \cos\theta) \tag{31}$$

4.4 Superposition

Considering now the case when there is a constant electric field with direction in z-axis simultaneously with a dielectric sphere of radius R having its center at the same origin of the coordinates. The potential at a given point M has two components, one originated by electric field E_0 and the second originated by the electric dipole due to the polarization of the spherical dielectric particle. We will cosider that the total potential has the form of the superposition of the two components described above:

$$V_{out} = Ar\cos\theta + Bf(r,\cos\theta) \qquad and \qquad V_{in} = Cr\cos\theta + Df(r,\cos\theta)$$

where A, B, C and D are constants that are calculated by means of the application of the boundary conditions. It is required that the potential at $r \to \infty$ should be the potential created by the constant electric field E_0 as the other terms vanish. This means that $A = -E_0$. Furthermore, the potential when $r \to 0$ should not tend to infinity, hence $D = 0$

$$V_{out} = -E_0 r\cos\theta + Bf(r,\cos\theta) \qquad and \qquad V_{in} = Cr\cos\theta \tag{32}$$

The two addictional boundary conditions required to calculate the constants B and C are that the potential inside and outside are the same at the sphere surface as there is no charge (potential is continuous) , and that the displacement flux vector D is continuous at the surface. So at $r = R$,

$$V_{out} = V_{in} \qquad and \qquad \varepsilon_m \frac{\partial V_{out}}{\partial r} = \varepsilon_p \frac{\partial V_{in}}{\partial r} \tag{33}$$

where ε_m is the permittivity of the medium and ε_p is the permittivity of the particle. Substituting in the equations (33) the equations (32), we find,

$$\begin{cases} -E_0 R\cos\theta + Bf(r,\cos\theta) &= CR\cos\theta \\ \varepsilon_m[-E_0\cos\theta + Bf'(r,\cos\theta)] &= \varepsilon_p C\cos\theta \end{cases} \tag{34}$$

where

$$f' = \frac{\partial f}{\partial r} = \frac{-\frac{2r - d\cos\theta}{2d\sqrt{r^2+(\frac{d}{2})^2 - rd\cos\theta}}}{r^2 + (\frac{d}{2})^2 - rd\cos\theta} - \frac{-\frac{2r + d\cos\theta}{2d\sqrt{r^2+(\frac{d}{2})^2 + rd\cos\theta}}}{r^2 + (\frac{d}{2})^2 + rd\cos\theta}$$

Solving the system, we find that

$$\begin{cases} C &= \frac{\varepsilon_m\left(E_0\cos\theta - RE_0\cos\theta\frac{f'}{f}\right)}{\varepsilon_m R\cos\theta\frac{f'}{f} - \varepsilon_p\cos\theta} \\ B &= RE_0\cos\theta\left[\frac{1}{f} + \frac{\cos\theta - R\cos\theta\frac{f'}{f}}{R\cos\theta\frac{f'}{f} - f\frac{\varepsilon_p}{\varepsilon_m}\cos\theta}\right] \end{cases} \tag{35}$$

Now, knowing that

$$V_{out-dip} = Bf = \frac{P}{4\pi\varepsilon_0} f \tag{36}$$

we can calculate an effective dipole P_{eff} as,

$$P_{eff} = 4\pi\varepsilon_0 B = 4\pi\varepsilon_0 R E_0 \cos\theta \left[\frac{1}{f} + \frac{\cos\theta - R\cos\theta\frac{f'}{f}}{R\cos\theta\frac{f'}{f} - f\frac{\varepsilon_p}{\varepsilon_m}\cos\theta}\right] \tag{37}$$

In this manner, we can say that the electric field is

$$E = -\nabla V = \vec{r}\left[E_0\cos\theta - \frac{P_{eff}}{4\pi\varepsilon_0}\frac{\partial f}{\partial r}\right] + \vec{t}\left[-E_0\sin\theta - \frac{P_{eff}}{4\pi\varepsilon_0}\frac{\partial f}{\partial t}\right] \tag{38}$$

where

$$\frac{\partial f}{\partial t} = \frac{\partial f}{\partial\theta}\frac{\partial\theta}{\partial t} = \frac{1}{r}\frac{\partial f}{\partial\theta} = \left[\frac{\frac{\sin\theta}{2\sqrt{r^2+(\frac{d}{2})^2-rd\cos\theta}}}{r^2+(\frac{d}{2})^2-rd\cos\theta} - \frac{-\frac{\sin\theta}{2\sqrt{r^2+(\frac{d}{2})^2+rd\cos\theta}}}{r^2+(\frac{d}{2})^2+rd\cos\theta}\right] \tag{39}$$

Figures (20), (21) and (22) show an example of the radial and tangential components of the electric field at a distance $r = 10 * R$ with $R = 180nm$, and of the module. All three magnitudes are plotted as a function of the angle θ

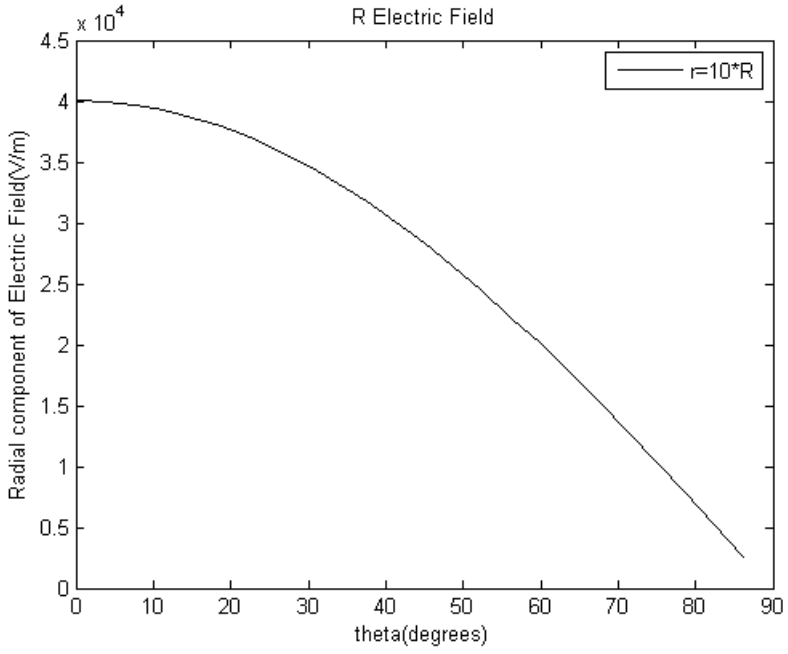

Figure 20: Radial component of Electric field

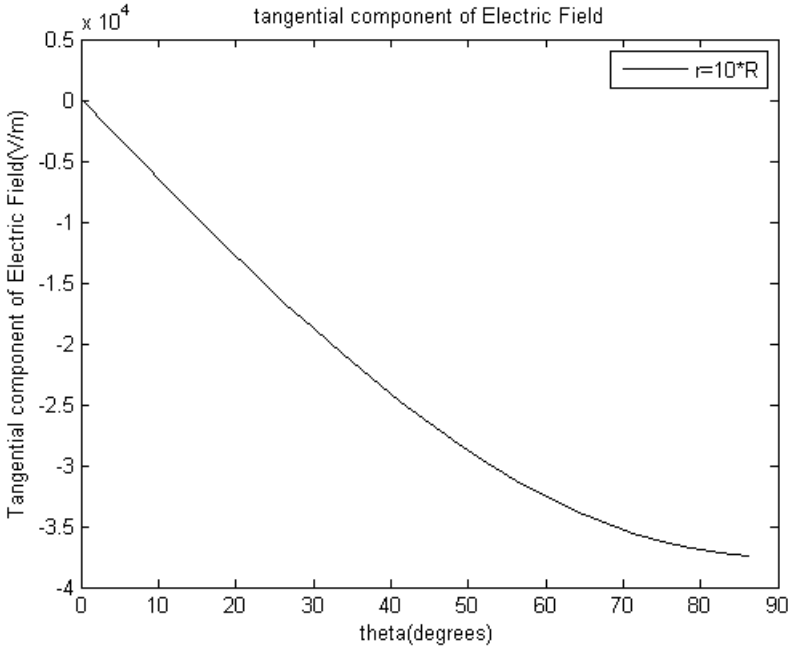

Figure 21: Tangential component of Electric field

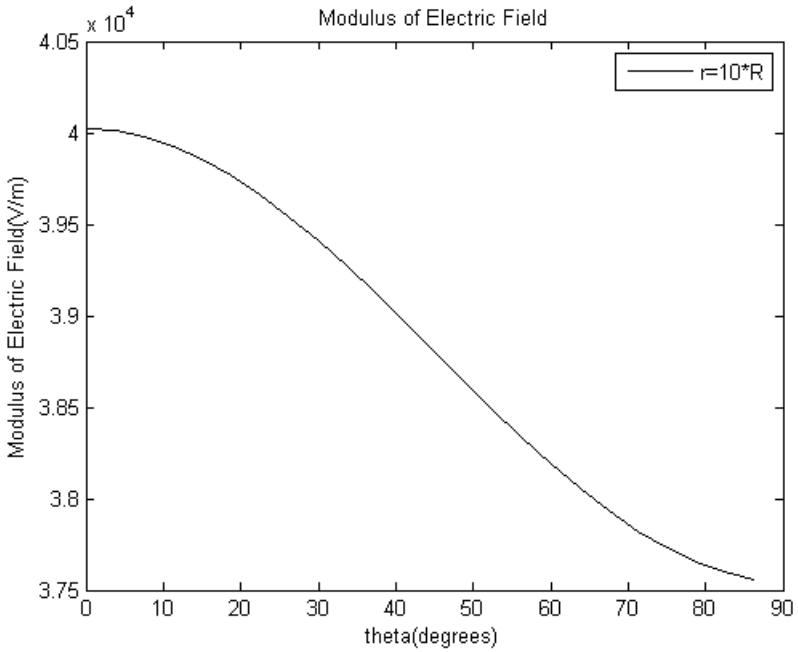

Figure 22: Modulus Electric field

Once the electric field is known we can calculate the force exerted on a second particle located at the distance r from the center at an angle θ using the effective moment model.

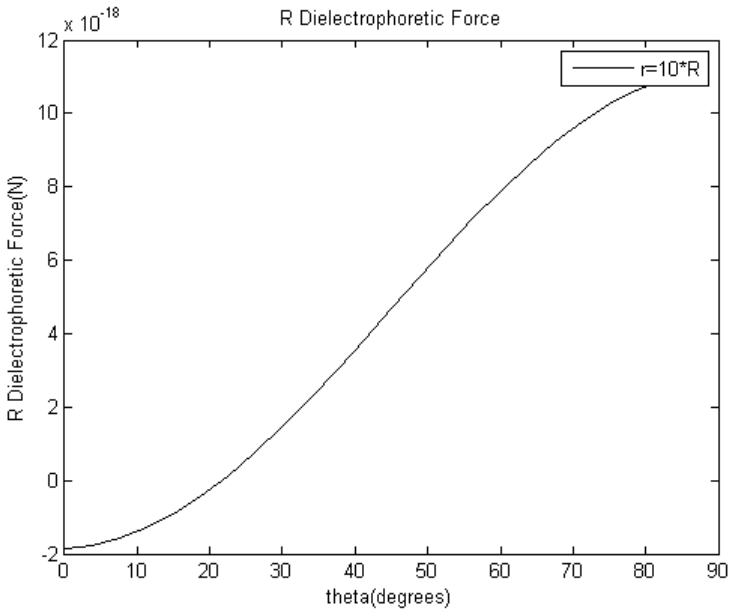

Figure 23: Dielectrophoretic force radial direction

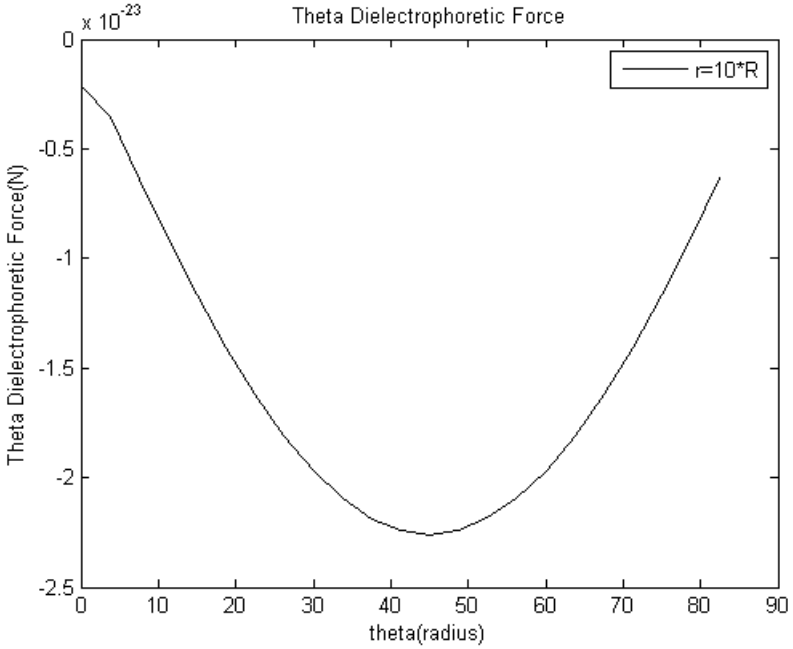

Figure 24: Dielectrophoretic force tangential direction

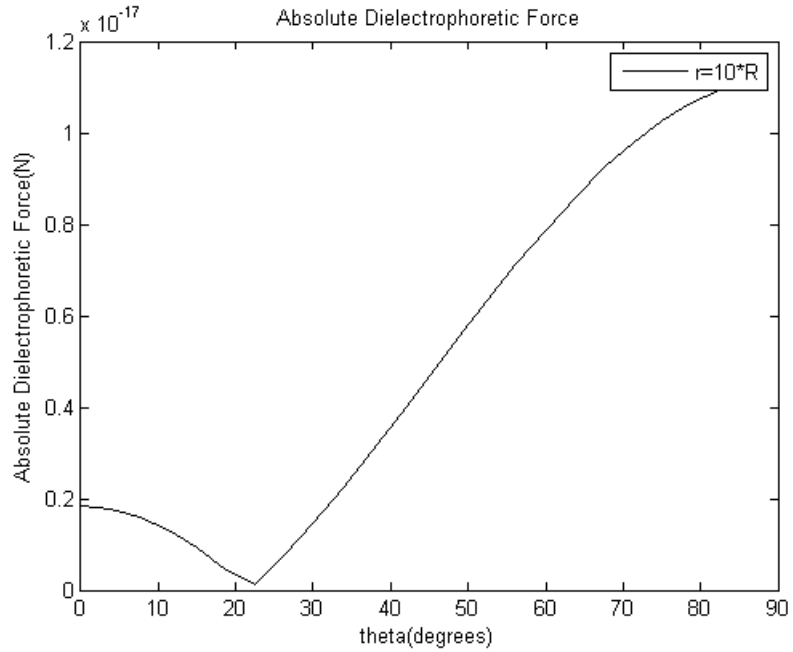

Figure 25: Modulus dielectrophoretic force

For more clarification, we show the direction of the Dielectrophoretic force in different angle position.

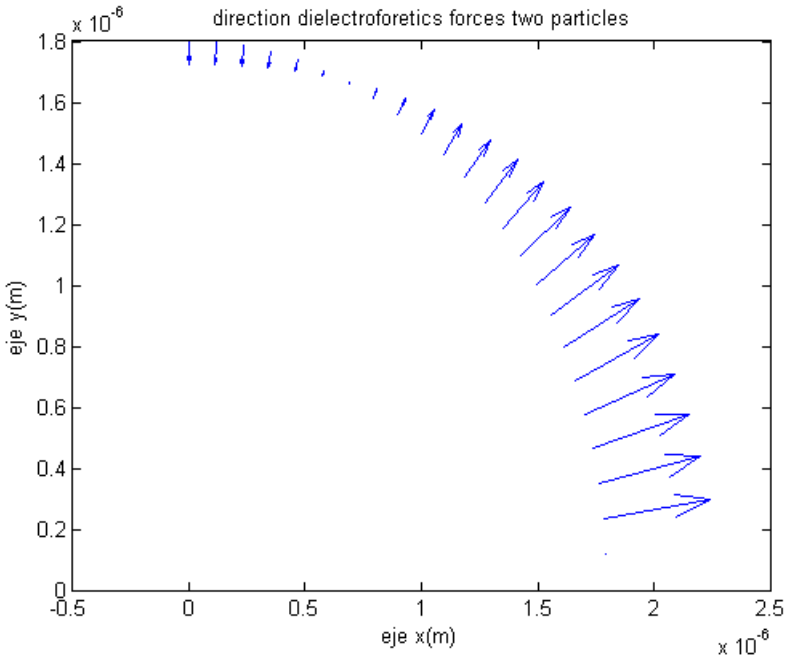

Figure 26: Behaviour of the force in changing angle

We can interpret the result by looking into the direction of the force vectors in figure (26), where we can see that the force is attractive in an angle of $\pm 25°$around the vertical position, whereas is repulsive for all other angles. This is consistent with the theory described in [25].

5 3D Dielectrophoretic force field

In order to understand better the behavior of the nanospheres when they are going to glide on the ground plane, we simulate on a three dimensional case an incoming particle that approaches to three fixed particle placed in triangular shape.

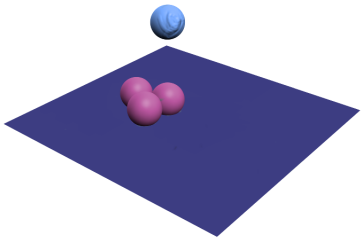

Figure 27: 3D scheme

5.1 Calculation in a simple case

First of all, we assume that the particle is located exactly in the vertical of the middle of the triangle. This is the simplest case talking about calculation level. Since the particle arrived from the center of the triangle, we notice that the distances between the incoming particle and the fixed particle are always the same and inversely proportional to the elevation angle.

$$r_3 = \frac{d}{\sqrt{3}\sin\theta} \tag{40}$$

In order to evaluate the total force due for each particle, we use the following formulas, obtained using the property of the tetrahedron:

$$F_{depx} = -F_{dep}\sin\theta\cos\left(\frac{\pi}{6}\right) + F_{dep}\sin\theta\cos\left(\frac{\pi}{6}\right) \tag{41}$$

$$F_{depy} = -F_{dep}\sin\theta\sin\left(\frac{\pi}{6}\right) + F_{dep}\sin\theta\sin\left(\frac{\pi}{6}\right) + F_{dep}\sin\theta \tag{42}$$

$$F_{depz} = F_{dep}\cos\theta + F_{dep}\cos\theta + F_{dep}\cos\theta \tag{43}$$

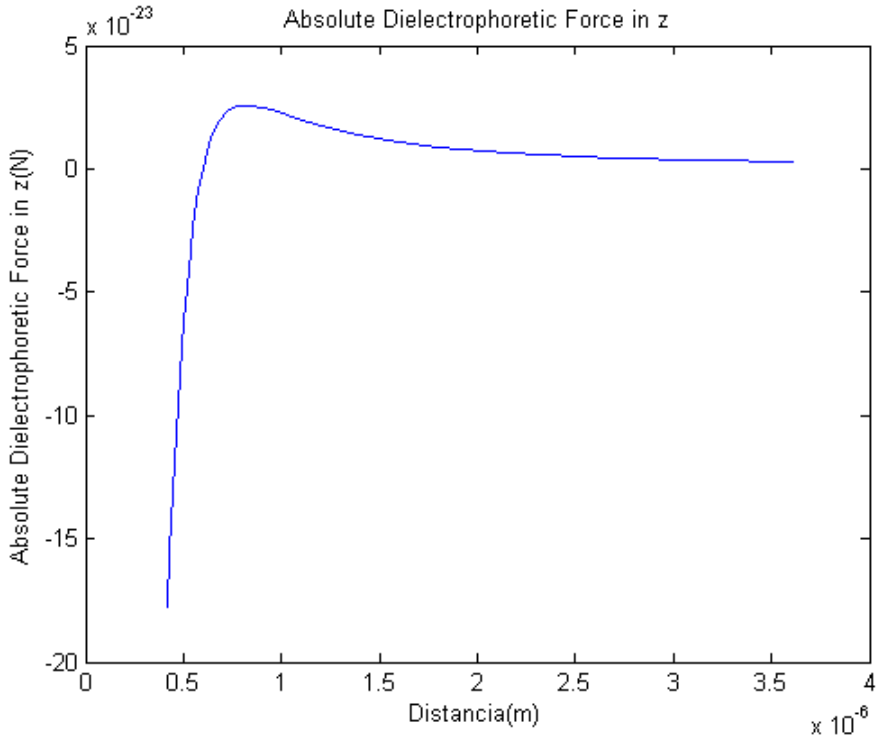

Figure 28: Resulting dielectrophoretic force in Z direction

The component in the x-axis and y-axis are negligeable due to the symmetry considered and the component in the direction of the z-axis as a transition from positive to negative at a given distance between the incoming particle and the three particles on the bottom substrate.

5.2 Obtain the others positions by Euler's angle

Once we have calculated the force in the simplified geometry, any other direction can be calculated using the Euler's angle rotation: yaw(ψ), pitch(θ) and roll(ϕ), used also in aeronautic [26] [27].

$$\begin{pmatrix} F_{depx}* \\ F_{depy}* \\ F_{depz}* \end{pmatrix} = \begin{bmatrix} \cos\psi\cos\theta\cos\phi - \sin\psi\sin\phi & \cos\psi\cos\theta\sin\phi + \sin\psi\cos\phi & -\cos\psi\sin\theta \\ -\sin\psi\cos\theta\cos\phi - \cos\psi\sin\phi & -\sin\psi\cos\theta\sin\phi + \cos\psi\cos\phi & \sin\psi\cos\theta \\ \sin\theta\cos\phi & \sin\theta\sin\phi & \cos\theta \end{bmatrix} \begin{pmatrix} F_{depx} \\ F_{depy} \\ F_{depz} \end{pmatrix}$$

The equation above extrapolate three new cartesian coordinates relative to the rotation of the three angles. In the figures (29) and (30) show the forces in each position of the moving particle in the case that we have a distance relatively small.

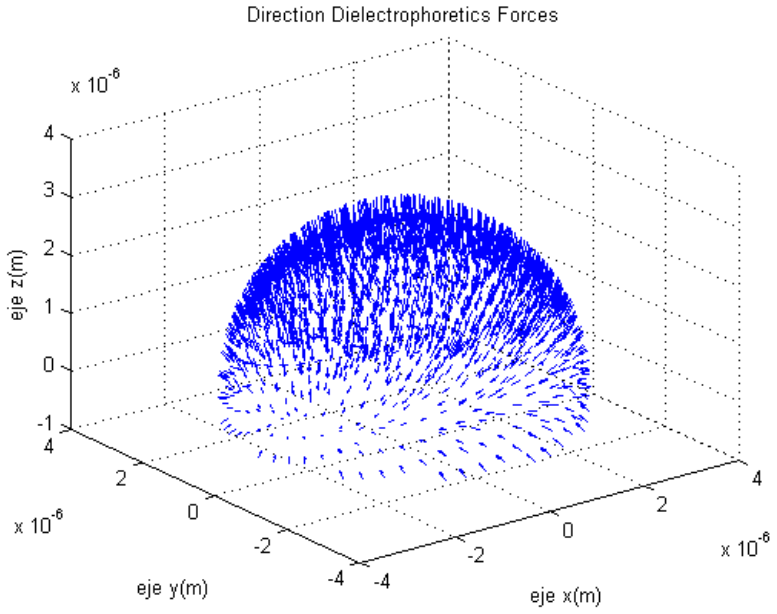

Figure 29: 3D actractive forces

We can notice that we have a change of direction of the forces when the distance between the particles become larger than $5.56 * 10^{-7}m$, so greater than 3 times the radius.

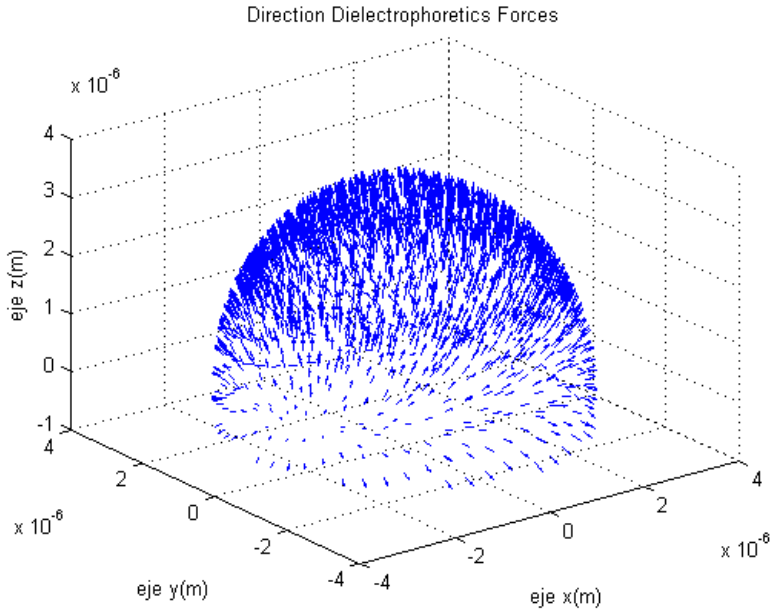

Figure 30: 3D repulsive forces

In order to calculate the influence of the Dielectrophoretic force in our system, let calculate the Weight force, using the formula (44),

$$\begin{aligned} V_{sphere} &= \frac{4}{3}\pi r_{cm}^3 \\ M_{ns} &= \frac{V_{sphere}\rho}{1000} \\ F_{weight} &= M_{ns}g \end{aligned} \tag{44}$$

where V_{sphere} is the volume of the nanosphere, r_{cm} is the radius of the nanosphere in cm, M_{ns} is the mass of the nanosphere in Kg, ρ is the density of the polystyrene $\left(\rho = 1.05\frac{g}{cm^3}\right)$, F_{weight} is the Weight force in N and g is the gravity acceleration, equal to $9.81\frac{m}{s^2}$. With those formulas we obtain a Weight force equal to $2.5 * 10^{-16}N$. Comparing it to the Dielectrophoretic force, that it is of the order of 10^{-23}, how we can see in the figure (28), we notice that the weight force is higher then the Dielectrophoretic force and hence a combination of these forces : weight in the downwards direction and the DEP force of varying direction are partly responsible for the experimental evidence. In this work we have concentrated on the DEP force only.

6 Conclusions

How we had saw in the pasts chapters, there are three main forces working in our system: the Coulomb force, the Weight force and the Dielectrophoretic force. With the data that we have extrapolated, we can derived those hypotesis:

1. At the beginning, when the droplets get outside the *conejet*, the nanospheres are wet, so the main force is the Coulomb one, toward the substrate (figures (14) (16));

2. When the particle are dried, the Coulomb force is zero, so the main force that acts in this conditions is the weight force;

3. When the particle land to the substrate, the Coulomb force still zero and the Dielectrophoretic force, with the combination of other forces like gravitational and hidrodynamic forces, explain the self- assembly saw in the empirical experiments [24].

A MATLAB CODE with explanation

```
%****************************
% schwartz-christofell model
%****************************
%Made by Davide Padoan- Universitat Politecnica de Catalunya/ Politecnico
%di Torino
%calculate the field distribution in a confiiguration electrode
%short-plane following the equations explicated in Appl. Phys Letts ,
%92, 173902(2008) by T.SUn, N.G. Green H.Morgan de la Universidad de
%Southampton

%DATOS
clear all;
h=10e-2;%it's the double of the distance needle-plane
h1=8e-2;
h2=12e-2;
w1=0.1e-3;
d11=4.995e-2;
d21=4.995e-2;
w2=0.5e-3;
d12=4.975e-2;
d22=4.975e-2;
w=0.3e-3;%width of the needle(diameter)
d1=4.985e-2;%half distance end to end edge of flat plate collector to ground
d2=4.985e-2;%the same but on the other side
V=10000;%potential applied at the needle, the plane is the ground
D=360e-9;%diameter of the particle
R=D/2;%radius of the particle
epsilon_vacuum=8.854187817e-12; %vacuum permittivity
epsilon_polystyrene=2.65*epsilon_vacuum;%polystirene permittivity
epsilon_air=1.00058986*epsilon_vacuum;%air permittivity

dist_max=20*R;%distance between particles
dist_10=10*R;%distance between particles



%complex plane T, every values are in the real axis
TA=0;
TB=1;
TC=1.0009;

eq1=h/(2*(d1+w+d2));

%Hilberg's approximation
if eq1>=1
    M= (0.25*exp(h*pi/(2*(d1+d2+w))));
    k1= (M-1)/(M+1);

else
    M= 0.25*exp(2*pi*(d1+d2+w)/h);
```

```
    k1= sqrt(1-((M-1)/(M+1))^2);
end
m=k1^2;
TF= (TB*(TC-TA)*k1^2-TA*(TC-TB))/((TC-TA)*k1^2-(TC-TB));
Kk=ellipke(m); %complete elliptical integral K(k1)


C3=h/(2*Kk);

a=0+1i*d2/C3;

[Sni,Cni,Dni]=ellipji(a,m,0.01); %call the ellipji.m file that give the
                                 %three elliptical functions, we needs only
                                 %sn and cn

b=0+ 1i*(w+d2)/C3;
[Snibis ,Cnibis,Dnibis]=ellipji(b,m,0.01);

TE= TF*TC*Cni^2/(TC-TF*Sni^2);
TD=TF*TC*Cnibis^2/(TC-TF*Snibis^2);

k2=sqrt((TE-TD)*(TF-TC)/((TF-TD)*(TE-TC)));
k2prima=sqrt(1-k2^2);
m2=k2prima^2;
Kk2prima=ellipke(m2);

field=2*V/h;



Zx=linspace(0,5e-2,100);
Zy=linspace(0,(d1+d2+w),100);



z=1;
while(z<=100)
    c=1;
    while (c<=100)
        Z=Zx(c)+1i*Zy(z);
        [SnT(c,z),CnT(c,z),DnT(c,z)]=ellipji(Z/C3,m,0.00000000001);
        T(c,z)=(TF*TC*(CnT(c,z))^2)/(TC-TF*(SnT(c,z))^2);
        E_0(c,z)=(conj(1i*(2*V/h)*(Kk/Kk2prima)*((TF-TD)^(0.5)*...
        (TE-TC)^(0.5)/((TF-TB)^(0.5)*(TC-TA)^(0.5)))*((T(c,z)-TB)^(0.5)*...
        (T(c,z)-TA)^(0.5)/((T(c,z)-TD)^(0.5)*(T(c,z)-TE)^(0.5)))));
        c=c+1;
    end
    z=z+1;
end

eqh1=h1/(2*(d1+w+d2));

%Hilberg's approximation
if eqh1>=1
```

```
    M= (0.25*exp(h1*pi/(2*(d1+d2+w))));
    k1= (M-1)/(M+1);

else
    M= 0.25*exp(2*pi*(d1+d2+w)/h1);
    k1= sqrt(1-((M-1)/(M+1))^2);
end
m=k1^2;
TF= (TB*(TC-TA)*k1^2-TA*(TC-TB))/((TC-TA)*k1^2-(TC-TB));
Kk=ellipke(m); %complete elliptical integral K(k1)


C3=h1/(2*Kk);

a=0+1i*d2/C3;

[Sni,Cni,Dni]=ellipji(a,m,0.01); %call the ellipji.m file that give the
                                 %three elliptical functions, we needs only
                                 %sn and cn

b=0+ 1i*(w+d2)/C3;
[Snibis ,Cnibis,Dnibis]=ellipji(b,m,0.01);

TE= TF*TC*Cni^2/(TC-TF*Sni^2);
TD=TF*TC*Cnibis^2/(TC-TF*Snibis^2);

k2=sqrt((TE-TD)*(TF-TC)/((TF-TD)*(TE-TC)));
k2prima=sqrt(1-k2^2);
m2=k2prima^2;
Kk2prima=ellipke(m2);

field=2*V/h1;

Zxh1=linspace(0,4e-2,100);



z=1;
while(z<=100)
    c=1;
    while (c<=100)
        Z=Zxh1(c)+1i*Zy(z);
        [SnT(c,z),CnT(c,z),DnT(c,z)]=ellipji(Z/C3,m,0.00000000001);
        T(c,z)=(TF*TC*(CnT(c,z))^2)/(TC-TF*(SnT(c,z))^2);
        E_0h1(c,z)=(conj(1i*(2*V/h1)*(Kk/Kk2prima)*((TF-TD)^(0.5)*...
        (TE-TC)^(0.5)/((TF-TB)^(0.5)*(TC-TA)^(0.5)))*((T(c,z)-TB)^(0.5)*...
        (T(c,z)-TA)^(0.5)/((T(c,z)-TD)^(0.5)*(T(c,z)-TE)^(0.5)))));
        c=c+1;
    end
    z=z+1;
end

eqh21=h2/(2*(d1+w+d2));
```

```
%Hilberg's approximation
if eqh21>=1
    M= (0.25*exp(h2*pi/(2*(d1+d2+w))));
    k1= (M-1)/(M+1);

else
    M= 0.25*exp(2*pi*(d1+d2+w)/h2);
    k1= sqrt(1-((M-1)/(M+1))^2);
end
m=k1^2;
TF= (TB*(TC-TA)*k1^2-TA*(TC-TB))/((TC-TA)*k1^2-(TC-TB));
Kk=ellipke(m); %complete elliptical integral K(k1)


C3=h2/(2*Kk);

a=0+1i*d2/C3;

[Sni,Cni,Dni]=ellipji(a,m,0.01); %call the ellipji.m file that give the
                                 %three elliptical functions, we needs only
                                 %sn and cn

b=0+ 1i*(w+d2)/C3;
[Snibis ,Cnibis,Dnibis]=ellipji(b,m,0.01);

TE= TF*TC*Cni^2/(TC-TF*Sni^2);
TD=TF*TC*Cnibis^2/(TC-TF*Snibis^2);

k2=sqrt((TE-TD)*(TF-TC)/((TF-TD)*(TE-TC)));
k2prima=sqrt(1-k2^2);
m2=k2prima^2;
Kk2prima=ellipke(m2);

field=2*V/h2;

Zxh2=linspace(0,6e-2,100);



z=1;
while(z<=100)
    c=1;
    while (c<=100)
        Z=Zxh2(c)+1i*Zy(z);
        [SnT(c,z),CnT(c,z),DnT(c,z)]=ellipji(Z/C3,m,0.00000000001);
        T(c,z)=(TF*TC*(CnT(c,z))^2)/(TC-TF*(SnT(c,z))^2);
        E_0h2(c,z)=(conj(1i*(2*V/h2)*(Kk/Kk2prima)*((TF-TD)^(0.5)*...
        (TE-TC)^(0.5)/((TF-TB)^(0.5)*(TC-TA)^(0.5)))*((T(c,z)-TB)^(0.5)*...
        (T(c,z)-TA)^(0.5)/((T(c,z)-TD)^(0.5)*(T(c,z)-TE)^(0.5)))));
        c=c+1;
    end
    z=z+1;
end
```

```
eqw11=h/(2*(d11+w1+d21));

%Hilberg's approximation
if eqw11>=1
    M= (0.25*exp(h*pi/(2*(d11+d21+w1))));
    k1= (M-1)/(M+1);

else
    M= 0.25*exp(2*pi*(d11+d21+w1)/h);
    k1= sqrt(1-((M-1)/(M+1))^2);
end
m=k1^2;
TF= (TB*(TC-TA)*k1^2-TA*(TC-TB))/((TC-TA)*k1^2-(TC-TB));
Kk=ellipke(m); %complete elliptical integral K(k1)


C3=h/(2*Kk);

a=0+1i*d21/C3;

[Sni,Cni,Dni]=ellipji(a,m,0.01); %call the ellipji.m file that give the
                                 %three elliptical functions, we needs only
                                 %sn and cn


b=0+ 1i*(w1+d21)/C3;
[Snibis ,Cnibis,Dnibis]=ellipji(b,m,0.01);

TE= TF*TC*Cni^2/(TC-TF*Sni^2);
TD=TF*TC*Cnibis^2/(TC-TF*Snibis^2);

k2=sqrt((TE-TD)*(TF-TC)/((TF-TD)*(TE-TC)));
k2prima=sqrt(1-k2^2);
m2=k2prima^2;
Kk2prima=ellipke(m2);

field=2*V/h;



Zx=linspace(0,5e-2,100);
Zy1=linspace(0,(d11+d21+w1),100);



z=1;
while(z<=100)
    c=1;
    while (c<=100)
        Z=Zx(c)+1i*Zy(z);
        [SnT(c,z),CnT(c,z),DnT(c,z)]=ellipji(Z/C3,m,0.00000000001);
        T(c,z)=(TF*TC*(CnT(c,z))^2)/(TC-TF*(SnT(c,z))^2);
        E_0w1(c,z)=(conj(1i*(2*V/h)*(Kk/Kk2prima)*((TF-TD)^(0.5)*...
        (TE-TC)^(0.5)/((TF-TB)^(0.5)*(TC-TA)^(0.5)))*((T(c,z)-TB)^(0.5)*...
```

```
        (T(c,z)-TA)^(0.5)/((T(c,z)-TD)^(0.5)*(T(c,z)-TE)^(0.5)))));
        c=c+1;
    end
    z=z+1;
end

eqw21=h/(2*(d12+w2+d22));

%Hilberg's approximation
if eqw21>=1
    M= (0.25*exp(h*pi/(2*(d12+d22+w2))));
    k1= (M-1)/(M+1);

else
    M= 0.25*exp(2*pi*(d12+d22+w2)/h);
    k1= sqrt(1-((M-1)/(M+1))^2);
end
m=k1^2;
TF= (TB*(TC-TA)*k1^2-TA*(TC-TB))/((TC-TA)*k1^2-(TC-TB));
Kk=ellipke(m); %complete elliptical integral K(k1)


C3=h/(2*Kk);

a=0+1i*d22/C3;

[Sni,Cni,Dni]=ellipji(a,m,0.01); %call the ellipji.m file that give the
                                 %three elliptical functions, we needs only
                                 %sn and cn

b=0+ 1i*(w2+d22)/C3;
[Snibis ,Cnibis,Dnibis]=ellipji(b,m,0.01);

TE= TF*TC*Cni^2/(TC-TF*Sni^2);
TD=TF*TC*Cnibis^2/(TC-TF*Snibis^2);

k2=sqrt((TE-TD)*(TF-TC)/((TF-TD)*(TE-TC)));
k2prima=sqrt(1-k2^2);
m2=k2prima^2;
Kk2prima=ellipke(m2);

field=2*V/h;



Zx=linspace(0,5e-2,100);
Zy2=linspace(0,(d12+d22+w2),100);



z=1;
while(z<=100)
    c=1;
    while (c<=100)
```

```
        Z=Zx(c)+1i*Zy(z);
        [SnT(c,z),CnT(c,z),DnT(c,z)]=ellipji(Z/C3,m,0.00000000001);
        T(c,z)=(TF*TC*(CnT(c,z))^2)/(TC-TF*(SnT(c,z))^2);
        E_0w2(c,z)=(conj(1i*(2*V/h)*(Kk/Kk2prima)*((TF-TD)^(0.5)*...
        (TE-TC)^(0.5)/((TF-TB)^(0.5)*(TC-TA)^(0.5)))*((T(c,z)-TB)^(0.5)*...
        (T(c,z)-TA)^(0.5)/((T(c,z)-TD)^(0.5)*(T(c,z)-TE)^(0.5)))));
        c=c+1;
    end
    z=z+1;
end

figure(20)
plot(Zy,abs(E_0h1(62,:)),'-b',Zy,abs(E_0(50,:)),'-r',Zy,abs(E_0h2(42,:)),'-g');
legend('h=8cm','h=10cm','h=12cm')
title('Behaviour Electric Field with h variation (measured in 2.5 cm)');
xlabel('Distance(m)');
ylabel('Absolute Electric Field(V/m)');

figure(21)
plot(Zy,abs(E_0w1(50,:)),'-b',Zy,abs(E_0(50,:)),'-r',Zy,abs(E_0w2(50,:)),'-g');
legend('w=0.1mm','w=0.3mm','w=0.5mm')
title('Behaviour Electric Field with w variation (measured in 2.5 cm)');
xlabel('Distance(m)');
ylabel('Absolute Electric Field(V/m)');


EA=abs(E_0);
figure(1)
plot(Zy,EA(20,:),'-b',Zy,EA(30,:),'-g',Zy,EA(40,:),'-r',Zy,EA(50,:),'-m',...
Zy,EA(60,:),'-c',Zy,EA(70,:),'-y',Zy,EA(80,:),'-k');
legend('1 cm','1.5 cm', '2 cm','2.5 cm', '3 cm','3.5 cm','4 cm');
title('Absolute Electric Field of the system')
xlabel('Distance(m)')
ylabel('Absolute Electric Field(V/m)')

figure(17)
plot(Zx,EA(:,50),'-b');
legend('On the needle');
title('Absolute Electric Field of the system')
xlabel('Distance h(m)')
ylabel('Absolute Electric Field(V/m)')



figure(19)
plot(Zy,EA(1,:),'-b');
legend('0.05 cm');
title('Absolute Electric Field near the needle')
xlabel('Distance(m)')
ylabel('Absolute Electric Field(V/m)')

E_cone=EA(100,50);%electric field at 500um

[gradEx1,gradEy1]=gradient(EA);
```

```
[gradEx,gradEy]=gradient(EA^2);

%we change the sign of the equations because the Matlab's gradient no take
%care of that
c=1;
while c<=50
    gradEx1(:,c)=-gradEx1(:,c);
    gradEy1(:,c)=-gradEy1(:,c);
    gradEx(:,c)=-gradEx(:,c);
    gradEy(:,c)=-gradEy(:,c);
    c=c+1;
end;

figure(18)
plot(Zx,gradEx1(:,50),'-b');
legend('On the needle');
title('Electric Field gradient on the needle')
xlabel('Distance h(m)')
ylabel('Electric Field gradient(V/m)')


Fdepx=2*pi*epsilon_air*R^3*((epsilon_polystyrene-epsilon_air)/...
(epsilon_polystyrene+2*epsilon_air))*gradEx;
Fdepy=2*pi*epsilon_air*R^3*((epsilon_polystyrene-epsilon_air)/...
(epsilon_polystyrene+2*epsilon_air))*gradEy;

%taylor's cone and droplet charge

ro=1000;%Kg/m^3
Vagua=73e-3;
theta=43.5;
Utt=0.863*sqrt(Vagua*h/epsilon_vacuum);
Ut=0.6791*sqrt(0.02275*h/epsilon_vacuum);
flow_rate=6.1e-10;%m^3/s
rdrop=(ro/(4*pi^2*Vagua*tan(pi/2-theta)*((V/Ut)^2-1)))^(1/3)*...
      flow_rate^(2/3);
Q=8*pi*sqrt(epsilon_air*V*rdrop^3);
FA=Q*EA;
Fx=Q*real(E_0);
Fy=Q*imag(E_0);
Fdep=abs(Fdepx+1i*Fdepy);
figure(2)
plot(Zy,FA(50,:),'-b',Zy,FA(60,:),'-g',Zy,FA(70,:),'-r',...
Zy,FA(80,:),'-m',Zy,FA(90,:),'-c',Zy,FA(100,:),'-k')

title('Absolute Coulomb Force for a single particle')
legend('2.5 cm','3 cm','3.5 cm','4 cm','4.5 cm','5 cm');
xlabel('Distance(m)')
ylabel('Absolute Coulomb Force(N)')

figure(3)
plot(Zy,Fdep(70,:),'-b',Zy,Fdep(80,:),'-g',Zy,Fdep(90,:),'-r',...
    Zy,Fdep(100,:),'-k')
```

```
legend('3.5 cm','4 cm','4.5 cm','5 cm')
title('Absolute Dielectrophoretic Force for a single particle')
xlabel('Distance(m)')
ylabel('Absolute Dielectrophoretic Force(N)')

figure(15)
quiver(Zy,Zx,Fy,Fx)
title('Coulomb Forces direction');
xlabel('Distance(m)');
ylabel('Distance(m)');

figure(16)
quiver(Zy,Zx, Fdepy,Fdepx);
title('Dielectrophoretic Forces direction');
xlabel('Distance(m)');
ylabel('Distance(m)');

%_____
%calculation of force between two particles

rd=linspace(0,dist_10,26); %distance between two particles
r=linspace(0,dist_10,25);

alphad=linspace(0,pi/2,26); %angle between two particles
alpha=linspace(0,pi/2,25);
k=(epsilon_polystyrene-epsilon_air)/...%Clausius Mossati Factor
(epsilon_polystyrene+2*epsilon_air);

z=1;
while(z<=25)
    c=1;
    while (c<=26)
        f_xt(c,z)=(1/D)/(sqrt(r(z)^2+(D^2)/4-r(z)*D*cos(alphad(c))))-...
            (1/D)/(sqrt(r(z)^2+(D^2)/4+r(z)*D*cos(alphad(c))));
        f_dr_xt(c,z)=-((2*r(z)-D*cos(alphad(c)))/(2*D*sqrt(r(z)^2+...
            (D^2)/4-r(z)*D*cos(alphad(c)))))/(r(z)^2+(D^2)/4-...
            r(z)*D*cos(alphad(c)))+((2*r(z)+D*cos(alphad(c)))/...
            (2*D*sqrt(r(z)^2+(D^2)/4+r(z)*D*cos(alphad(c)))))/...
            (r(z)^2+(D^2)/4+r(z)*D*cos(alphad(c)));
        c=c+1;
    end
    z=z+1;
end
z=1;
while(z<=26)
    c=1;
    while (c<=25)
        f_xr(c,z)=(1/D)/(sqrt(rd(z)^2+(D^2)/4-rd(z)*D*cos(alpha(c))))-...
            (1/D)/(sqrt(rd(z)^2+(D^2)/4+rd(z)*D*cos(alpha(c))));
        f_dr_xr(c,z)=-((2*rd(z)-D*cos(alpha(c)))/(2*D*sqrt(rd(z)^2+...
            (D^2)/4-rd(z)*D*cos(alpha(c)))))/(rd(z)^2+(D^2)/4-...
            rd(z)*D*cos(alpha(c)))+((2*rd(z)+D*cos(alpha(c)))/...
            (2*D*sqrt(rd(z)^2+(D^2)/4+rd(z)*D*cos(alpha(c)))))/...
            (rd(z)^2+(D^2)/4+rd(z)*D*cos(alpha(c)));
```

```
        c=c+1;
    end
    z=z+1;
end



c=1;
while (c<=26)
    Pb_xr(c,:)=4.*pi.*epsilon_vacuum.*R.*EA(100,50).*cos(alpha).*...
        (1./f_xr(:,c)'+ (cos(alpha)-(R.*cos(alpha).*...
        f_dr_xr(:,c)')./f_xr(:,c)')./(R.*cos(alpha).*f_dr_xr(:,c)'-...
        (epsilon_polystyrene./epsilon_air).*f_xr(:,c)'.*cos(alpha)));
    V_xr(c,:)=(Pb_xr(c,:)./(4.*pi.*epsilon_vacuum)).*f_xr(:,c)';
    c=c+1;
end;

c=1;
while (c<=25)
    E_r_t(:,c)=diff(V_xr(:,c))./(dist_10/25);%we have a change of the sign
                                             %caused by the Matlab's
                                             %derivation
    c=c+1;
end;

c=1;
while (c<=25)
    E_r(:,c)=(EA(100,50).*cos(alpha))' + E_r_t(c,:)';
    Pb_xt(c,:)=4.*pi.*epsilon_vacuum.*R.*EA(100,50).*cos(alphad).*...
        (1./f_xt(:,c)'+ (cos(alphad)-(R.*cos(alphad).*...
        f_dr_xt(:,c)')./f_xt(:,c)')./(R.*cos(alphad).*f_dr_xt(:,c)'-...
        (epsilon_polystyrene./epsilon_air).*f_xt(:,c)'.*cos(alphad)));
    V_xt(c,:)=(Pb_xt(c,:)./(4.*pi.*epsilon_vacuum)).*f_xt(:,c)';
    E_alpha_sin_r(c,:)=-diff(V_xt(c,:))./(pi/2/25);
    E_alpha(c,:)=-(EA(100,50).*sin(alpha))+E_alpha_sin_r(c,:)./r(c);
    c=c+1;
end;

E_abs=sqrt(E_r.^2+E_alpha'.^2);
[gradEr,gradEalpha]=gradient(E_abs.^2);
Fdepr=2.*pi.*epsilon_air.*R.^3.*k.*gradEr./(dist_10/25);
Fdepalpha=2.*pi.*epsilon_air.*R.^3.*k.*gradEalpha./(pi/2/25);

c=1;
while (c<=25)
    z=1;
    while (z<=25)
        if Fdepr(c,z)>0
            phi(c,z)=atan(Fdepalpha(c,z)/Fdepr(c,z));
        else
            phi(c,z)=atan(Fdepalpha(c,z)/Fdepr(c,z))+pi;
        end;
        z=z+1;
    end;
```

```
    c=c+1;
end;
asx=r(25).*sin(alpha);
asy=r(25).*cos(alpha);
Fx=sqrt(Fdepr(:,25)'.^2+Fdepalpha(:,25)'.^2).*cos((pi/2-alpha-phi(:,25)'));
Fy=sqrt(Fdepr(:,25)'.^2+Fdepalpha(:,25)'.^2).*sin((pi/2-alpha-phi(:,25)'));




figure(14)
quiver(asx,asy,Fx,Fy);
title('direction dielectroforetics forces two particles')

ylabel('eje y(m)')
xlabel('eje x(m)')

Fdepabs=sqrt(Fdepr.^2+Fdepalpha.^2);

alphag=alpha.*180/pi;
figure(4)
plot(alphag,E_r(:,25),'-k')
legend('r=10*R')
title('R Electric Field')
xlabel('theta(degrees)')
ylabel('Radial component of Electric Field(V/m)')
figure(5)
plot(alphag,E_alpha(25,:),'-k')
legend('r=10*R')
title('tangential component of Electric Field')
xlabel('theta(degrees)')
ylabel('Tangential component of Electric Field(V/m)')
figure(6)
plot(alphag,E_abs(:,25),'-k')
legend('r=10*R')
title('Modulus of Electric Field')
xlabel('theta(degrees)')
ylabel('Modulus of Electric Field(V/m)')
figure(7)
plot(alphag,Fdepr(:,25),'-k')
legend('r=10*R')
title('R Dielectrophoretic Force')
xlabel('theta(degrees)')
ylabel('R Dielectrophoretic Force(N)')
figure(8)
plot(alphag,Fdepalpha(:,25),'-k')
legend('r=10*R')
title('Theta Dielectrophoretic Force')
xlabel('theta(radius)')
ylabel('Theta Dielectrophoretic Force(N)')
figure(9)
plot(alphag,Fdepabs(:,25),'-k')
legend('r=10*R')
```

```
title('Absolute Dielectrophoretic Force')
xlabel('theta(degrees)')
ylabel('Absolute Dielectrophoretic Force(N)')
figure(10)
angle=(alpha'+(pi/2-phi(:,25))).*180/pi;
plot(alphag,angle,'-k')
title('phi angle')
xlabel('theta(degrees)')
ylabel('phi(degrees)')

%------
%calculation forces between 3 to 1 (3D) with particle in the middle
%distance 20*R
alpha_min=atan(sqrt(3)/30);

alpha_max=atan(sqrt(3)/3);
alpha=linspace(alpha_min,alpha_max,25); %angle between two particles
alphad=linspace(alpha_min,alpha_max,26); %angle between two particles
alphadd=linspace(alpha_min,alpha_max,27); %angle between two particles
alphag=alpha.*180/pi;
R_cm=R*10^2; %Radius in cm
Volume_sphere=4/3*pi*R_cm^3;
dens=1.05; % density polystirene in g/cm^3
weight=Volume_sphere*dens/1000; %in kg
F_weight=weight*9.81;
c=1;
while (c<=25)
    r3g(c)=D*sqrt(3)/(3*sin(alpha(c)));%distance between spheres
    c=c+1;
end;
c=1;
while (c<=26)
    r3(c)=D*sqrt(3)/(3*sin(alphad(c)));%distance between spheres
    c=c+1;
end;
c=1;
while (c<=27)
    rd3(c)=D*sqrt(3)/(3*sin(alphadd(c)));%distance between spheres
    c=c+1;
end;
z=1;
while(z<=27)
    c=1;
    while (c<=27)
        if z==28-c
        f(c)=(1/D)/(sqrt(rd3(z)^2+(D^2)/4-rd3(z)*D*cos(alphadd(c))))-...
            (1/D)/(sqrt(rd3(z)^2+(D^2)/4+rd3(z)*D*cos(alphadd(c))));
        f_dr(c)=-((2*rd3(z)-D*cos(alphadd(c)))/(2*D*sqrt(rd3(z)^2+...
            (D^2)/4-rd3(z)*D*cos(alphadd(c)))))/(rd3(z)^2+(D^2)/4-...
            rd3(z)*D*cos(alphadd(c)))+((2*rd3(z)+D*cos(alphadd(c)))/...
            (2*D*sqrt(rd3(z)^2+(D^2)/4+rd3(z)*D*cos(alphadd(c)))))/...
            (rd3(z)^2+(D^2)/4+rd3(c)*D*cos(alphadd(c)));
        end;
        c=c+1;
```

```
    end
    z=z+1;
end


Pb=4.*pi.*epsilon_vacuum.*R.*EA(100,50).*cos(alphadd).*(1./f+...
    (cos(alphadd)-(R.*cos(alphadd).*f_dr)./f)./(R.*cos(alphadd).*f_dr-...
    (epsilon_polystyrene./epsilon_air).*f.*cos(alphadd)));
V=(Pb./(4.*pi.*epsilon_vacuum)).*f;
E_r_t=D.*cos(alphad).*sqrt(3)./(3.*sin(alphad).^2).*diff(V)./...
    (abs(alpha(25)-alpha(1))/25);
E_r3=(EA(100,50).*cos(alphad)) + E_r_t;
E_alpha_sin_r=-diff(V)./(abs(alpha(25)-alpha(1))/25);
E_alpha3=-(EA(100,50).*sin(alphad))+E_alpha_sin_r./r3;
E_abs3=sqrt(E_alpha3.^2+E_r3.^2);

gradEr3=-D.*cos(alpha).*sqrt(3)./(3.*sin(alpha).^2).*diff(E_abs3.^2)./...
    (abs(alpha(25)-alpha(1))/25);
gradEalpha3=diff(E_abs3.^2)./(abs(alpha(25)-alpha(1))/25);
Fdepalpha3=2*pi*epsilon_air*R^3*k*gradEalpha3;
Fdepr3=2*pi*epsilon_air*R^3*k*gradEr3;
Fdepabs3=sqrt(Fdepalpha3.^2+Fdepr3.^2);
c=1;
while (c<=25)
    if Fdepr3(c)>0
        phi3(c)=atan(Fdepalpha3(c)/Fdepr3(c));
    else
        phi3(c)=atan(Fdepalpha3(c)/Fdepr3(c))+pi;
    end;
    c=c+1;
end;
Fdepx=(-Fdepabs3.*sin(alpha)*cos(pi/6)+Fdepabs3.*sin(alpha)*...
    cos(pi/6)).*cos(pi/2-alpha+phi3);
Fdepy=(-Fdepabs3.*sin(alpha)*sin(pi/6)-Fdepabs3.*sin(alpha)*sin(pi/6)+...
    Fdepabs3.*sin(alpha)).*cos(pi/2-alpha+phi3);
Fdepz=(Fdepabs3.*cos(alpha)+Fdepabs3.*cos(alpha)+Fdepabs3.*cos(alpha)).*...
    sin(pi/2-alpha+phi3);
Fdep_dip_xy=Fdepabs3.*cos(pi/2-alpha+phi3);
Fdep_dip_z=Fdepabs3.*sin(pi/2-alpha+phi3);
alphag=alpha.*180./pi;

figure(11)
plot(r3g,Fdepx)
title('Absolute Dielectrophoretic Force in x')
xlabel('Distancia(m)')
ylabel('Absolute Dielectrophoretic Force in x(N)')

figure(12)
plot(r3g,Fdepy)
title('Absolute Dielectrophoretic Force in y')
xlabel('Distancia(m)')
ylabel('Absolute Dielectrophoretic Force in y(N)')

figure(13)
```

```
plot(r3g,Fdepz)
title('Absolute Dielectrophoretic Force in z')
xlabel('Distancia(m)')
ylabel('Absolute Dielectrophoretic Force in z(N)')


%threshold electric field
k_b=1.3806488*10^(-23);%Boltzmann's constant
T=300;% Room temperature in Kelvin
Eth=1.7*R^(-3/2)*sqrt(k_b*T/epsilon_air)/k;




%1 to 3 with moving particle using Euler's angles
asse_x=1;
asse_y=2;
asse_z=3;
yaw=linspace(-pi/4,pi/4,12);%(psi)
pitch=linspace(-pi/4,pi/4,12);%(theta)
roll=linspace(-pi,pi,12);%(phi)
angolo=17; %5

[Y, RO]=meshgrid(yaw,roll);

Fdep1=[-Fdep_dip_xy(angolo).*sin(alpha(angolo)).*cos(pi/6+pi/3);...
    -Fdep_dip_xy(angolo).*sin(alpha(angolo)).*sin(pi/6+pi/3);...
    Fdep_dip_z(angolo).*cos(alpha(angolo))];
Fdep2=[-Fdep_dip_xy(angolo).*sin(alpha(angolo)).*sin(pi/3);...
    Fdep_dip_xy(angolo).*sin(alpha(angolo)).*cos(pi/3);...
    Fdep_dip_z(angolo).*cos(alpha(angolo))];
Fdep3=[Fdep_dip_xy(angolo).*sin(alpha(angolo)).*cos(pi/3);...
    -Fdep_dip_xy(angolo).*sin(alpha(angolo)).*sin(pi/3);...
    Fdep_dip_z(angolo).*cos(alpha(angolo))];

F1x=Fdep1(asse_x);
F1y=Fdep1(asse_y);
F1z=Fdep1(asse_z);
F2x=Fdep2(asse_x);
F2y=Fdep2(asse_y);
F2z=Fdep2(asse_z);
F3x=Fdep3(asse_x);
F3y=Fdep3(asse_y);
F3z=Fdep3(asse_z);


[P, RO]=meshgrid(pitch,roll);
%cambio coordinate
k=1;
while k<=12
    l=1;
    while l<=12
        g=1;
```

```
        while g<=12
            Fdep1Ex(g,l,k)=((cos(yaw(g)).*cos(pitch(l)).*cos(roll(k))-...
                sin(yaw(g)).*sin(roll(k)))+...
                sin(yaw(g)).*cos(pitch(l)).*cos(roll(k))+...
                cos(yaw(g)).*sin(roll(k))-...
                sin(pitch(l)).*cos(roll(k))).*F1x;
            Fdep1Ey(g,l,k)=((-cos(yaw(g)).*cos(pitch(l)).*sin(roll(k))-...
                sin(yaw(g)).*cos(roll(k)))-...
                sin(yaw(g)).*cos(pitch(l)).*sin(roll(k))+...
                cos(yaw(g)).*cos(roll(k))+...
                sin(pitch(l)).*sin(roll(k))).*F1y;
            Fdep1Ez(g,l,k)=(cos(yaw(g)).*sin(pitch(l))+...
                sin(yaw(g)).*sin(pitch(l)) + cos(pitch(l))).*F1z;
            Fdep2Ex(g,l,k)=((cos(yaw(g)).*cos(pitch(l)).*cos(roll(k))-...
                sin(yaw(g)).*sin(roll(k)))+...
                sin(yaw(g)).*cos(pitch(l)).*cos(roll(k))+...
                cos(yaw(g)).*sin(roll(k))-...
                sin(pitch(l)).*cos(roll(k))).*F2x;
            Fdep2Ey(g,l,k)=((-cos(yaw(g)).*cos(pitch(l)).*sin(roll(k))-...
                sin(yaw(g)).*cos(roll(k)))-...
                sin(yaw(g)).*cos(pitch(l)).*sin(roll(k))+...
                cos(yaw(g)).*cos(roll(k))+...
                sin(pitch(l)).*sin(roll(k))).*F2y;
            Fdep2Ez(g,l,k)=(cos(yaw(g)).*sin(pitch(l))+...
                sin(yaw(g)).*sin(pitch(l)) + cos(pitch(l))).*F2z;
            Fdep3Ex(g,l,k)=((cos(yaw(g)).*cos(pitch(l)).*cos(roll(k))-...
                sin(yaw(g)).*sin(roll(k)))+...
                sin(yaw(g)).*cos(pitch(l)).*cos(roll(k))+...
                cos(yaw(g)).*sin(roll(k))-...
                sin(pitch(l)).*cos(roll(k))).*F3x;
            Fdep3Ey(g,l,k)=((-cos(yaw(g)).*cos(pitch(l)).*sin(roll(k))-...
                sin(yaw(g)).*cos(roll(k)))-...
                sin(yaw(g)).*cos(pitch(l)).*sin(roll(k))+...
                cos(yaw(g)).*cos(roll(k))+...
                sin(pitch(l)).*sin(roll(k))).*F3y;
            Fdep3Ez(g,l,k)=(cos(yaw(g)).*sin(pitch(l))+...
                sin(yaw(g)).*sin(pitch(l)) + cos(pitch(l))).*F3z;
            g=g+1;
        end;
        l=l+1;
    end;
    k=k+1;
end;



k=1;
while k<=12
    l=1;
    while l<=12
        g=1;
        while g<=12
            X=[(cos(yaw(g)).*cos(pitch(l)).*cos(roll(k))-...
                sin(yaw(g)).*sin(roll(k))),...
```

```
                sin(yaw(g)).*cos(pitch(l)).*cos(roll(k))+...
                cos(yaw(g)).*sin(roll(k)),-sin(pitch(l)).*cos(roll(k));
               (-cos(yaw(g)).*cos(pitch(l)).*sin(roll(k))-...
               sin(yaw(g)).*cos(roll(k))),...
               -sin(yaw(g)).*cos(pitch(l)).*sin(roll(k))+...
               cos(yaw(g)).*cos(roll(k)),+sin(pitch(l)).*sin(roll(k));
                cos(yaw(g)).*sin(pitch(l)),+sin(yaw(g)).*sin(pitch(l)),...
                + cos(pitch(l))]'*10*R;
            FdeptotEx(g,l,k)=Fdep1Ex(g,l,k)+Fdep2Ex(g,l,k)+Fdep3Ex(g,l,k);
            FdeptotEy(g,l,k)=Fdep1Ey(g,l,k)+Fdep2Ey(g,l,k)+Fdep3Ey(g,l,k);
            FdeptotEz(g,l,k)=Fdep1Ez(g,l,k)+Fdep2Ez(g,l,k)+Fdep3Ez(g,l,k);

            ejex(g,l,k)=X(1,1)+X(2,1)+X(3,1);
            ejey(g,l,k)=X(1,2)+X(2,2)+X(3,2);
            ejez(g,l,k)=X(1,3)+X(2,3)+X(3,3);
            g=g+1;
        end;
        l=l+1;
    end;
    k=k+1;
end;


figure(47)
quiver3(ejex,ejey,ejez,FdeptotEx,FdeptotEy,FdeptotEz);
title('Direction Dielectrophoretics Forces');

zlabel('eje z(m)');
ylabel('eje y(m)');
xlabel('eje x(m)');
```

References

[1] R. Daz, S. Payen,*Biological cell separation using dielectrophoresis in a microfluidic device* , University of California, Berkeley, Bio and Thermal Engineering Laboratory EECS 245

[2] Blanca H. Lapizco-Encinas,Blake A. Simmons,Eric B. Cummings,Yolanda Fintschenko, *Insulator-based dielectrophoresis for the selective concentration and separation of live bacteria in water* ,Electrophoresis (2004), **25**, 16951704

[3] Soma Das, Mitali Saha,*Preparation of Carbon Nanosphere From Bamboo And Its Use In Water Purification*, Current Trends in Technology and Science, Volume : 2, Issue : 1 , **174-177** (2012)

[4] Jack W. Plunkett,*Plunkett's Nanotechnology & MEMS Industy Almanac*, (2013)

[5] Brandon K Chen, Yong Zhang, Doug D Perovic and Yu Sun,*MEMS microgrippers with thin gripping tips*, J. Micromech. Microeng. **21** (2011) 105004 (5pp)

[6] Frank Alexis, Eric M. Pridgen, Robert Langer, Omid C. Farokhzad *Nanoparticle Technologies for Cancer Therapy* M. Schafer-Korting (ed.), Drug Delivery, Handbook of Experimental Pharmacology 197, Springer-Verlag Berlin Heidelberg (2010)

[7] Product Info Sheet - Schoeller Textiles AG

[8] Pierre Colson, Catherine Henrist, and Rudi Cloots, *Nanosphere Lithography: A Powerful Method for the Controlled Manufacturing of Nanomaterials*, Journal of Nanomaterials, Volume 2013 (2013)

[9] Scriven, L.E. , *Physics and applications of dip coating and spin coating*,volume 121, pp. 717729, Materials Research Society (1988).

[10] Scriven, LE , *Physics and applications of dip coating and spin coating*, Materials Research Society proceedings 121, (1988)

[11] Xiaozhou Ye, Limin Qi, *Two-dimensionally patterned nanostructures based on monolayer colloidal crystals: Controllable fabrication, assembly, and applications*, Volume 6, Issue 6, Pages 608631 (2011)

[12] Matteo Albani and Filippo Capolino,*Wave dynamics by a plane wave on a half-space metamaterial made of plasmonic nanospheres: a discrete WienerHopf formulation*, J. Opt. Soc. Am. B / Vol. 28, No. 9 / September (2011)

[13] R Paniagua-Domnguez, F Lopez-Tejeira, R Marques and J A Sanchez-Gil,*Metallo-dielectric coreshell nanospheres as building blocks for optical three-dimensional isotropic negative-index metamaterials*, New Journal of Physics **13** (2011) 123017 (15pp)

[14] M. Lungu, A. Neculae, M. Bunoiu, N. Strambeanu, *Some considerationon the nanoparticles manipulation in fluid media using dielectrophoresis*, Rom. Journ. Phys., Vol. 56, Nos. 56, P. 749756, Bucharest, (2011)

[15] Malmstrm, David, *Nanoparticles in Capillary Electrophoresis hyphenated with Mass Spectrometry What are the benefits?* Department of Physical and Analytical chemistry. 38 pp. Uppsala (2011)

[16] Yun Wu, Anthony Duong, L. James Lee and Barbara E. Wyslouzil, *Electrospray Production of Nanoparticles for Drug/Nucleic Acid Delivery*, The Delivery of Nanoparticles, Dr. Abbass A. Hashim (Ed.), (2012)

[17] A. Jaworek, *Electrospray droplet sources for thin lm deposition*, J Mater Sci (2007) 42:266297

[18] T. Sun, N.G.Green, H.Morgan, *Analytical solution for the electric field and dielectrophoretic force in a dielectrophoretic focusing electrode structure*, Appl. Phys. Lett. **92**, 173901 (2008)

[19] R. Schinzinger and P. A. A. Laurra, *Conformal Mapping: Methods and Applications* , Dover, Mineola, New York, (2003)

[20] I.S. Gradshteyn and I.M.Ryzhik,*Table of integrals, Series and products*, 5th ed. Academic, San Diego, New York, (1994)

[21] W. Hilberg, *IEEE Trans. Microwave Theory Tech.* **17**, 259(1969)

[22] Chitral J. Angammana and SheSha H. Jayaram, *Investigation of the Optimum Electric Field for a Stable electrospinning Process*, IEEE TRANSACTIONS ON INDUSTRY APPLICATIONS, VOL 48, NO. 2, MARCH/APRIL (2012)

[23] Matthias S. Wilm and Matthias Mann, *Electrospray and Taylor-cone theory, Dole's beam of macromolecules at last?*, International Journal of Mass Spectrometry and Ion Processes 136 (1994), 167-180

[24] Arnau Coll, Sandra Bermejo, Luis Castañer, *Self-assembly of ordered silica nanostructures by electrospray*, to be published

[25] Thomas B. Jones, *Basic Theory of Dielectrophoresis and Electrorotation*, IEEE ENGINEERING IN MEDICINE AND BIOLOGY MAGAZINE, november/december (2003)

[26] O.M. OReilly. *Intermediate Dynamics for Engineers: a Unied Treatment of Newton-Euler and Lagrangian Mechanics*, Cambridge University Press (2008).

[27] David Eberly, *Euler Angle Formulas* ,Geometric Tools, LLC (2014)